ASSESSMENT OF COMPONENT LEVEL TRITIUM TRANSPORT FOR FISSION AND FUSION SYSTEMS

A Thesis Presented for the

Master of Science

Degree

The University of Tennessee, Knoxville

Miles Landon O'Neal

August 2021

ACKNOWLEDGEMENTS

Foremost, I would like to extend my sincerest gratitude to my supervisor, Professor Nicholas R. Brown, for his continuous support of my thesis study and research, for his guidance and mentorship, and for his investment in my development as a nuclear engineer. Besides my supervisor, I would like to thank Dr. Seokbin Seo for his assistance on the use of BISON and his technical knowledge. His continued support was fundamental towards the completion of this work.

Additionally, I would like to thank the rest of my thesis committee: Professor Ivan G. Maldonado and Professor David C. Donovan. Their time and participation are greatly valued and appreciated. Also, I am highly indebted to the faculty and staff of the University of Tennessee who so generously gave me their time and knowledge, which I was able to apply to the completion of this endeavor.

I am also grateful to my family for their support. Throughout my life they have pushed me forward and have instilled in me the values that have led me here. They have been a key motivator to work hard towards my goals.

This work was supported by the US Department of Energy, Office of Fusion Energy Sciences under contract No. DE-AC05-00OR22725. This research made use of the resources of the High Performance Computing Center at Idaho National Laboratory, which is supported by the Office of Nuclear Energy of the U.S. Department of Energy and the Nuclear Science User Facilities under Contract No. DE-AC07-05ID14517. Portions of graduate studies were supported by a Penn State IRP funded by the U.S. Department of Energy.

ABSTRACT

Tritium transport behavior in component-level models of fission and fusion systems was simulated and assessed using the hydrogen transport code in the BISON fuel performance code. Models of different conditions which were of an ITER heat exchanger, LWR cladding, and FHR heat exchanger were conducted. Comparable results between reported values and BISON predictions demonstrated the ability of the models to predict tritium transport behavior through different steel materials for three different model conditions. Next, a method for sensitivity and uncertainty analysis was implemented to calibrate the models as well as demonstrate the ability to apply this approach in multiphysics models in BISON. This calibration method resulted in improving BISON predictions. Overall, the capabilities of the BISON code for component-level modeling of tritium transport are promising and BISON predictions showed good agreement for the three cases.

TABLE OF CONTENTS

CHAPTER ONE INTRODUCTION 1

CHAPTER TWO LITERATURE REVIEW 9

Hydrogen Transport in BISON code 9

Assessment of Tritium Transport Parameters in Steels 12

Tritium Behavior in Fission Systems 20

Tritium Behavior in Breeding Blankets 23

CHAPTER THREE TRITIUM TRANSPORT MODELING OF STEEL STRUCTURES IN BISON 26

SS 316L Heat Exchanger for ITER 27

FeCrAl Cladding for an LWR 31

SS 316 Heat Exchanger for an FHR 34

CHAPTER FOUR SENSITIVITY ANALYSIS AND MODEL CALIBRATION 40

Calibration of ITER Heat Exchanger Model 44

Calibration of LWR Cladding Model 48

Calibration of FHR Heat Exchanger Model 51

CHAPTER FIVE CONCLUSIONS 59

REFERENCES 62

VITA 73

LIST OF TABLES

Table 1. Effective cross-sections for tritium producing reactions and precursors 2

Table 2. Composition of stainless steels 13

Table 3. Hydrogen isotope diffusivity in various steels, partially adapted from Dolan ... 14

Table 4. Values of tritium transport parameters for steel models in BISON..... 28

Table 5. Major parameter variation ranges for Sobol sensitivity analysis 42

LIST OF FIGURES

Figure 1. Diagram of modeling approach formulation. 7

Figure 2. Cross section of the FNSF 10

Figure 3. Comparison of diffusivity of hydrogen isotopes from multiple studies in (1) SS 304, (2) SS 316, and (3) SS 316L with solid, dashed, and dotted lines for hydrogen, deuterium, and tritium respectively. 16

Figure 4. Percent standard deviation of hydrogen isotope diffusion parameters for various stainless steels. 17

Figure 5. Percent standard deviation of diffusivity of hydrogen isotopes in (1) SS 304, (2) SS 316, (3) and SS 316L with solid, dotted, and dashed lines for hydrogen, deuterium, and tritium respectively 18

Figure 6. Schematic of BISON models of steel components. 21

Figure 7. Schematic of ITER heat exchanger tritium transport model in BISON. 30

Figure 8. Evolution of tritium distribution across the SS 316L heat exchanger wall..... 30

Figure 9. Schematic of tritium transport model in BISON of FeCrAl cladding. 33

Figure 10. Steady state temperature distribution in the x-direction. 33

Figure 11. Time evolving tritium distribution in FeCrAl cladding. 35

Figure 12. Tritium distribution in FeCrAl cladding at (1) 1000, (2) 5000, and (3) 120000 seconds. 36

Figure 13. Schematic of FHR heat exchanger tritium transport model in BISON. 38

Figure 14. Transient tritium concentration comparison between reported values and BISON predictions. 38

Figure 15. Sobol indices of input parameters for three steel models 45

Figure 16. Scatter plots of RMSE of tritium permeation rate through SS 316L heat exchanger 46

Figure 17. Scatter plot of RMSE of tritium concentration distribution across FeCrAl cladding 49

Figure 18. Time evolving tritium distribution in FeCrAl cladding. 49

Figure 19. Tritium distribution in FeCrAl cladding at (1) 1000, (2) 5000, and (3) 120000 seconds. 50

Figure 20. Scatter plot of RMSE of time dependent tritium concentration within a SS 316 heat exchanger 52

Figure 21. Transient tritium concentration comparison between reported values, initial BISON predictions, and BISON predictions that resulted in the smallest RMSE 54

Figure 22. Sobol indices of sampled parameters for FHR heat exchanger model with variable alpha boundary conditions. 56

Figure 23. Scatter plots of RMSE of time dependent tritium concentration within a SS 316 heat exchanger tube wall with variable alpha boundary conditions 57

Figure 24. Transient tritium concentration comparison between reported values, initial minimum RMSE, and improved minimum RMSE BISON predictions 58

CHAPTER ONE

INTRODUCTION

Nuclear energy, both fission and fusion, have the ability to provide large amounts of ultra-low carbon electricity [1]. With demand for energy expected to continue to grow, nuclear energy provides an important alternative to fossil fuels. Nuclear reactions require a multitude of considerations due to safety and economic needs. Tritium, a radioactive isotope of hydrogen with a half-life of 12.3 years, is a safety consideration and a key component of fuel for fusion reactors, and thereby, an economic consideration as well.

In both fission and fusion reactors, tritium production occurs due to nuclear reactions [2]. Considering light water reactors (LWRs), tritium is mostly produced as a product of ternary fission of uranium, though, it can also be created due to neutron activation reactions. This results in tritium production occurring in some materials used for control rods, burnable poisons, and reactor coolant. Table 1 lists some of these reactions and their effective microscopic cross-sections. For tritium to be released to the environment, it must first enter the coolant, and the rate this occurs depends on material selection of the cladding. Comparing the commonly used zirconium-based alloys with ferritic steels, zircaloy cladding have lower emission rates of tritium into the coolant [3]. Heavy water reactors (HWRs) produce tritium through the same reactions as LWRs, though, it is mostly produced as a result of neutron activation of deuterium in heavy water. Following production in the coolant, ternary fission of the fuel is the second most contributing mechanism.

Table 1. Effective cross-sections for tritium producing reactions and precursors [2].

Reaction	$\boldsymbol{\sigma_{eff}}$ $(\mathbf{10^{-28}}\ \boldsymbol{m^2})$
^{2}H(n,γ)T	0.000316
^{6}Li(n,α)T	693
^{7}Li(n,nα)T	0.0516
^{10}B(n,α)Li	3060
^{10}B(n,2α)T	1.27

Other reactor designs such as liquid metal fast breeder reactors (LMFBRs), molten salt breeder reactors (MSBRs), and high temperature gas cooled reactors (HTGRs) produce tritium through the same mechanisms as LWRs. Though contributions to overall production vary. LMFBRs, similar to LWRs, mostly produce tritium as a result of ternary fission followed by neutron activation of reactor components. Due to the use of lithium coolant for MSBRs, the primary production mechanism is rather neutron activation of the lithium coolant followed by ternary fission. Production in HTGRs results from ternary fission in the fuel, neutron activation of ^{3}He coolant, lithium impurities in the graphite moderator, and control element utilizing boron. From this, tritium clearly is produced in any fission reactor, however, their design has a significant impact on the amount, method, and location it is created.

The production of tritium in a commercial fusion reactor design, unlike the majority of fission reactor designs, is intentionally planned to occur and necessary for reactor performance [4-6]. Future fusion reactors are expected to utilize deuterium and tritium fusion:

$$D + T \rightarrow {}^{4}_{2}He + n + 17.6\ MeV \tag{1}$$

For tritium resources to be sufficient for a reactor to be economically acceptable, breeder blankets surround the reactor core, and are designed to produce slightly more tritium than used in the fusion process. This is done by utilizing neutrons produced from the fusion

reaction as well as neutron multiplier materials in the blanket such as Be or Pb to react with lithium in the blanket:

$$^{6}_{3}Li + n \rightarrow T + ^{4}_{2}He + 4.8\ MeV \tag{2}$$

$$^{7}_{3}Li + n \rightarrow T + ^{4}_{2}He + n - 2.5\ MeV \tag{3}$$

Whereas the necessity for more tritium to be produced than used is due to its natural scarcity, the natural loss through radioactive decay, and to buildup tritium inventory to start up new tritium projects like a new fusion reactor. This would also supply other important work such as research and development which utilizes tritium.

Blankets, in addition to producing tritium, fulfill the function of extracting the energy produced from the fusion reactor, and thereby, have a direct impact on the efficiency and economics of a reactor [4-6]. There are essentially two major types of fusion blankets which are liquid metal and solid breeders. Liquid breeder blanket designs include the Self Cooled Lithium Lead (SCLL), Water Cooled Lithium Lead (WCLL), and Dual Coolant Lead Lithium (DCLL) which utilize liquid PbLi eutectic as both the neutron multiplier and tritium breeder. The SCLL and DCLL use the PbLi as both a tritium breeder and coolant, though, the DCLL design also utilizes He coolant. In regards to the WCLL, the liquids main functionality is clearly divided with water as the coolant and PbLi as the tritium breeder. The Helium Cooled Pebble Bed (HCPB) blanket utilize solid pebbles of Li_4SiO_4 in tritium breeding regions, regions of solid neutron multiplier materials such as Be, and He as both coolant and purge gas. Purge gas is used to extract tritium produced in the breeding

regions. Liquid breeders have the advantage of no swelling or damage accumulation of the breeder as well as the adjustment of breeder composition outside the blanket to maintain tritium production. Though concerns with them arise from material considerations such as corrosion of coolant channels and low tritium solubility in PbLi as well as electromagnetic effects since the coolant is a metal.

As tritium readily permeates through most metals such as steel, its release to the environment from reactors poses a radiological concern. When tritium decays, it releases a low-energy beta particle and changes into helium-3. This beta particle does not pose an external radiological hazard as it is unable to penetrate the skin's outer layer; however, it can be an internal risk. Of particular concern is the ingestion of tritiated water due to it being readily absorbed by the body. Additionally, separation of tritium from water is difficult thereby making the contamination of water furthermore undesirable.

As per the guidance from the U.S. Department of Energy and NRC, tritium release to the environment must be regulated due to it being a radioactive isotope [7, 8]. Though tritium must be well controlled, it has multiple uses including one as fuel for fusion reactors. Considering its natural scarcity, an additional constraint on tritium inventory exists in which tritium will need to be produced for fusion energy and development to continue [9, 10]. Therefore, tritium transport and behavior must be accounted for due to safety and economic considerations.

The work in this thesis was conducted to evaluate component-level tritium transport modeling using BISON and its hydrogen transport code. Steel components were assessed due to its common use as a structural material for both fission and fusion

systems. To begin, studies of tritium transport in steels were chosen to assess BISON's ability to predict and calculate key results of tritium buildup and permeation in structural materials. Also, to consider expected reactor operation such as steady state and transients, studies with different temperature and tritium boundary conditions were selected. Figure 1 shows the formulation process of this work in which three different studies were modeled in BISON with increasing model complexity to systematically assess different model capabilities. First, the assessment of diffusion in BISON followed an ITER (International Thermonuclear Experimental Reactor) tritium permeation experiment of its heat exchanger where only Fick's diffusion is considered due to a constant temperature across the steel wall [11]. Second, an assessment of multiphysics followed a tritium transport model based off experimental work of a PWR FeCrAl cladding where steady state conditions were considered [12]. As the model had a temperature gradient across the cladding as a result of fission in the fuel, multiphysics was introduced since BISON considers the Soret effect and the temperature dependence of the diffusion coefficient. Third, an assessment of transients in BISON followed modeling work of an FHR heat exchanger where a startup transient causes tritium buildup in the primary coolant [13]. Multiphysics was still considered for this case due to a temperature gradient. Following this, a sensitivity study of these models was conducted to demonstrate a method for sensitivity analysis/uncertainty quantification (SA/UQ) as well as optimization/calibration of tritium transport modeling of nuclear reactor systems due to the large variance of diffusivity. This work aims to assess expanding the use of BISON code to include tritium transport of fission and fusion systems.

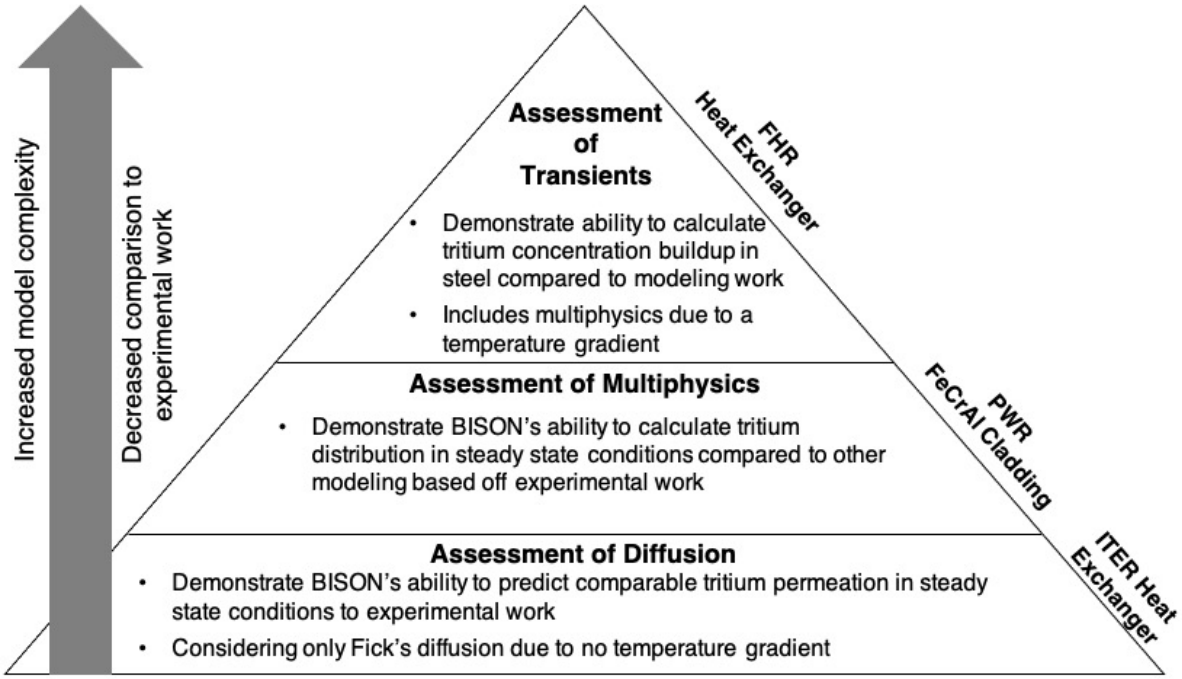

Figure 1. Diagram of modeling approach formulation.

Portions of the work presented in this thesis were previously published as a third author in two journal articles. One was published in the Journal of Nuclear Materials which was accepted on March 10, 2021 [14], and the other in Fusion Engineering and Design that was accepted on June 23, 2021 [15].

CHAPTER TWO

LITERATURE REVIEW

A literature review was conducted to understand the hydrogen transport code in BISON utilized to simulate tritium transport as well as tritium aspects of fission and fusion systems. Tritium production occurs in all fission reactors as a result of fission and neutron activation of tritium forming material [16, 17]. The reactors which produce more tritium than the more common light water reactors (LWR) are the heavy water and fast reactors [18, 19]. This production of tritium in fission reactors, specifically heavy water CANDU reactors, is a key tritium resource that fuels fusion development [10]. In regards to fusion reactors, tritium production occurs in the coolant blankets where it is created due to a reaction between neutrons released from the core and a form of lithium in the blanket [20]. One considered blanket design is the dual coolant lead lithium (DCLL) blanket which have inherent design features such as a relatively high PbLi flow rate that result in limiting tritium losses. A cross section of a fusion reactor design for a Fusion Nuclear Science Facility (FNSF) can be seen in Figure 2.

Hydrogen Transport in BISON code

BISON is based off of the Idaho National Laboratory (INL) Multiphysics Object-Oriented Simulation Environment (MOOSE) code which utilizes the finite element method to solve systems of coupled equations [21]. BISON can solve fully-coupled partial differential equations for heat transfer, species diffusion, and stress equilibrium for 3D

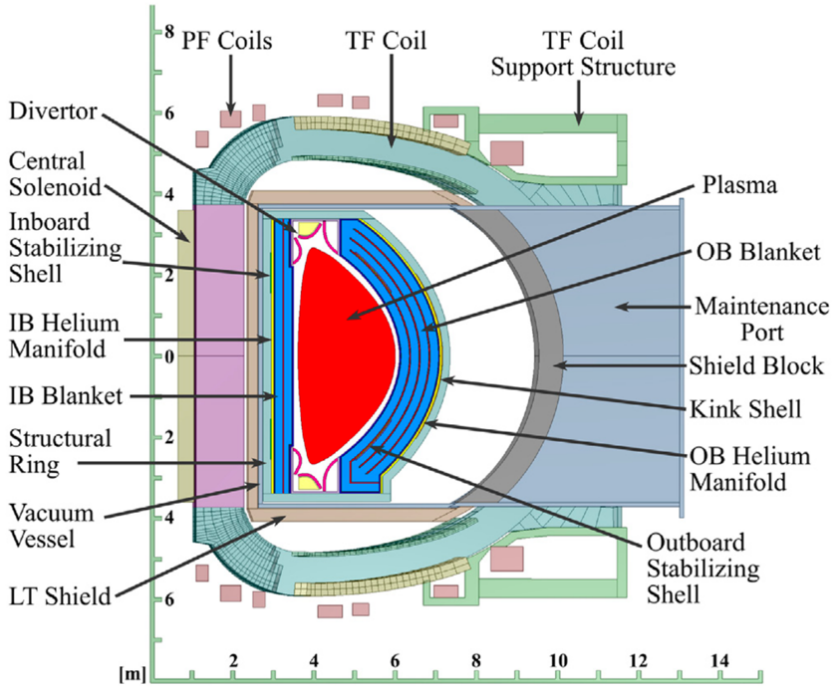

Figure 2. Cross section of the FNSF [20].

solids, 2D plane, and 1D layer geometries. BISON has the ability to extend modeling considerations to include a coupled multiphysics analysis of a system and to conduct high fidelity analysis of steady state and transient conditions. For example, considering a dual coolant lead lithium (DCLL) blanket, BISON would be able to conduct complex 3D as well as simple 1D tritium transport simulations coupled to a neutronic code like MCNP to provide tritium production information and a thermal-hydraulics code providing coolant flow conditions such as RELAP5-3D [22, 23].

Previous studies have worked to implement a hydrogen migration and redistribution model as well as verify and validate simulations by comparing to historic experimental data [24-28]. The hydrogen transport model in BISON considers two principal phenomena for hydrogen transport behavior in zirconium alloy fuel cladding, hydrogen diffusion in solid solution and hydride precipitation and dissolution. As tritium is a radioactive isotope of hydrogen, its transport behavior in metals is similar to hydrogen though parameter values require adjustment depending on the material it is diffusing through. In this study, the models are of steels which are non-hydride forming metals, and therefore, hydride precipitation and dissolution phenomena as well as their equations within BISON were not considered [29, 30]. Diffusion of tritium in solid solution is driven by a concentration gradient defined by Fick's law, J_{Fick}, and a temperature gradient known as the Soret effect, J_{Soret} [31-33]. The total tritium flux, J_{tot}, is therefore the sum of both contributions given by

$$J_{tot} = J_{Fick} + J_{Soret} = -D_H \nabla C_{ss} - \frac{D_H C_{ss} Q^*}{RT^2} \nabla T \tag{4}$$

where C_{ss} is the tritium concentration in solid solution in the metal, Q^* is the heat of transport in units of J/mol, D_H is the tritium diffusion coefficient of the metal in units of m^2/s, R is the ideal gas constant, and T is the temperature in Kelvin. The diffusion coefficient of tritium is dependent on temperature, and thus, defined by Arrhenius' Law [31-35]:

$$D_H = A_D \exp\left(-\frac{E_D}{RT}\right) \tag{5}$$

where A_D is the pre-exponential factor with units of m^2/s and E_D is the activation energy for diffusion of tritium in a metal with units of J/mol.

Assessment of Tritium Transport Parameters in Steels

A review of hydrogen isotope transport in various stainless steels was conducted to inform the tritium modeling and model calibration of chosen steel studies. The studies chosen were of steel structures using SS 316, SS 304, and SS 316L whose compositions are presented in table 2. From this, the makeup of the steels shows small differences, and explain why hydrogen isotope transport parameters were found to be comparable in many experiments. A report by Dolan et al. [33] reviewed studies of hydrogen interactions in steels where many diffusivity experiments of hydrogen isotopes were tabulated [36-47]. This review included additional studies of which the majority were more current studies into the diffusion coefficient, and are presented in table 3 [34, 48-50]. The methods

Table 2. Composition of stainless steels.

Element	SS 304	SS 316	SS 316L	SS 316LN
Fe	Balanced	Balanced	Balanced	Balanced
Cr	18.53	16.0-18.0	16.0-18.0	16.0-18.0
Mo	0.14	2.0-3.0	2.0-3.0	2.0-3.0
Mn	1.31	2.0	2.0	2.0
C	0.062	0.08	0.03	0.03
S	0.02	0.03	0.03	0.03
Si	0.57	0.75	0.75	1.0
P	-	0.045	0.045	0.045
Ni	-	10.0-14.0	10.0-14.0	10.0-14.0
N	-	0.1	0.1	0.1-0.3

Table 3. Hydrogen isotope diffusivity in various steels, partially adapted from Dolan [33].

Material	Isotope	Temperature Range (K)	A_d (J/mole)	E_d (m^2/s)	Reference
SS 304	H	600-1000	54892.82	1.200E-06	[37]
SS 304	H	812-1190	52095.12	9.960E-07	[39]
SS 304	H	373-873	54313.98	2.720E-06	[39]
SS 304	H	663-780	50744.50	3.200E-07	[42]
SS 304	H	373-623	53252.79	7.690E-07	[43]
SS 304	H	625-1000	49700.00	8.250E-07	[34]
SS 304	D	273-873	61935.31	1.800E-05	[36]
SS 304	D	300-400	58848.19	1.200E-05	[47]
SS 304	D	812-1190	50262.14	6.610E-07	[39]
SS 304, etc.	D	400-714	54024.57	3.400E-07	[41]
SS 304,316	D,T	298-500	51130.39	2.400E-07	[41]
SS 304,316	D,T	500-1173	59427.02	1.700E-06	[41]
SS 304	T	373-573	56725.79	1.240E-06	[39]
SS 304	T	298-498	58462.30	1.800E-06	[39]
SS 304	T	373-473	5691.87	7.200E-07	[41]
SS 304,316	T	298-495	60777.64	1.100E-06	[41]
SS 316	H	373-623	49300.00	2.010E-07	[51]
SS 316	H	588-1000	47800.00	6.320E-07	[34]
SS 316L	H	600-900	59716.44	2.990E-06	[44]
SS 316L	H	873-1173	54024.57	1.300E-06	[40]
SS 316L	H	623-1123	55100.00	1.240E-06	[49]
SS 316-ST1	H	423-723	46306.77	4.700E-07	[38]
SS 316LN	H	573-1123	56510.00	1.590E-06	[48]
SS 316L	D	600-900	58076.41	1.740E-06	[44]
SS 316L	D	623-1123	57500.00	1.380E-06	[49]
SS 316LN	D	573-1123	56800.00	1.380E-06	[48]
SS 316	T	603-853	63961.23	4.200E-06	[46]
SS 316	T	288-573	61300.00	1.900E-06	[50]
SS 316L	T	600-900	57883.46	1.410E-06	[44]
SS 316L	T	500-873	15146.17	2.300E-10	[45]

used in determining diffusivity include time-lag, thermal desorption, steady state permeation, and continuous-flow gas-phase permeation. Figure 3 shows diffusivity of hydrogen, deuterium, and tritium in SS 304, SS 316, and SS 316L where SS 316LN was assumed as SS 316L due to only small changes in composition.

From the initial review of diffusivity parameter values, the values varied across the different studies, steels, and hydrogen isotopes, and thus, prompted an investigation into the standard deviation of the experimental data. Without considering temperature, it was found that the largest source of uncertainty comes from the pre-exponential factor with the largest percent standard deviation being about 139% for deuterium in SS 304, as shown in Figure 4. The activation energy, though, also showed large variance in some cases such as about 58% for tritium in SS 316L.

Figure 5 presents the percent standard deviation of the diffusion coefficient dependent on temperature for SS 304, SS 316, and SS 316L for hydrogen, deuterium, and tritium. This resulted in large standard deviations for all three steels. Though, the steel, temperature, and hydrogen isotope influenced how large the standard deviation was. For SS 304, the values were largest for deuterium whereas the only comparable point for deuterium in SS 316 was below 5%. In regards to SS 316L, the standard deviation was noticeably small for hydrogen and deuterium across all temperatures considered, though, the deviation for tritium noticeably increased with temperature. From this, it can be determined that diffusivity of hydrogen isotope transport in steels has large uncertainty, and thereby, compel the use of model calibration to improve BISON predictions of study conditions.

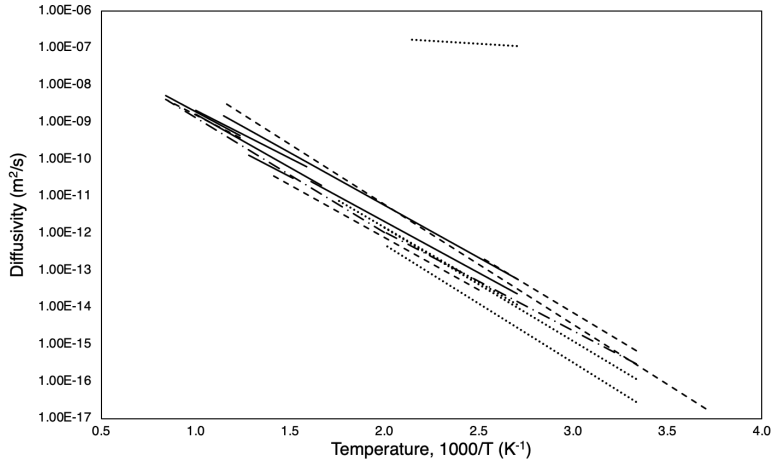

(1)

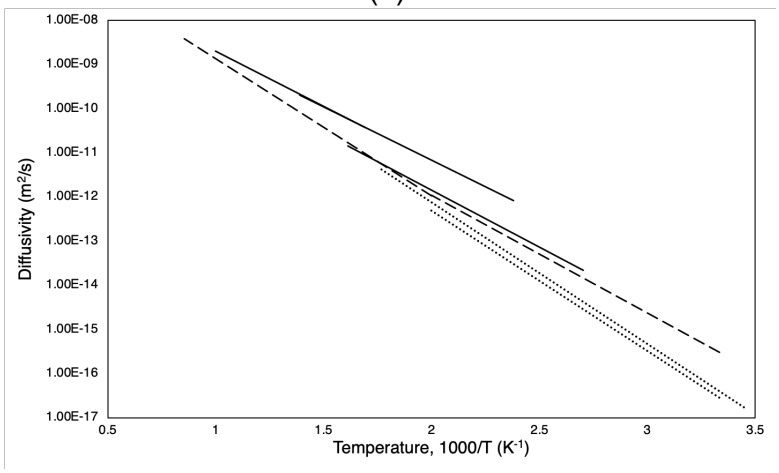

(2)

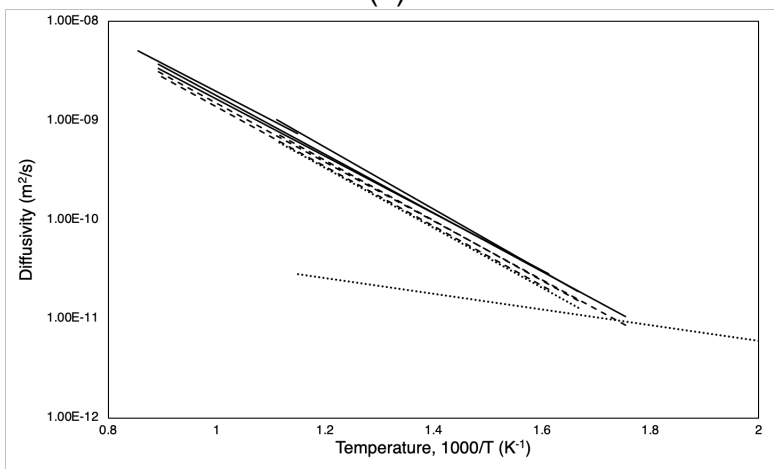

(3)

Figure 3. Comparison of diffusivity of hydrogen isotopes from multiple studies in (1) SS 304, (2) SS 316, and (3) SS 316L with solid, dashed, and dotted lines for hydrogen, deuterium, and tritium respectively.

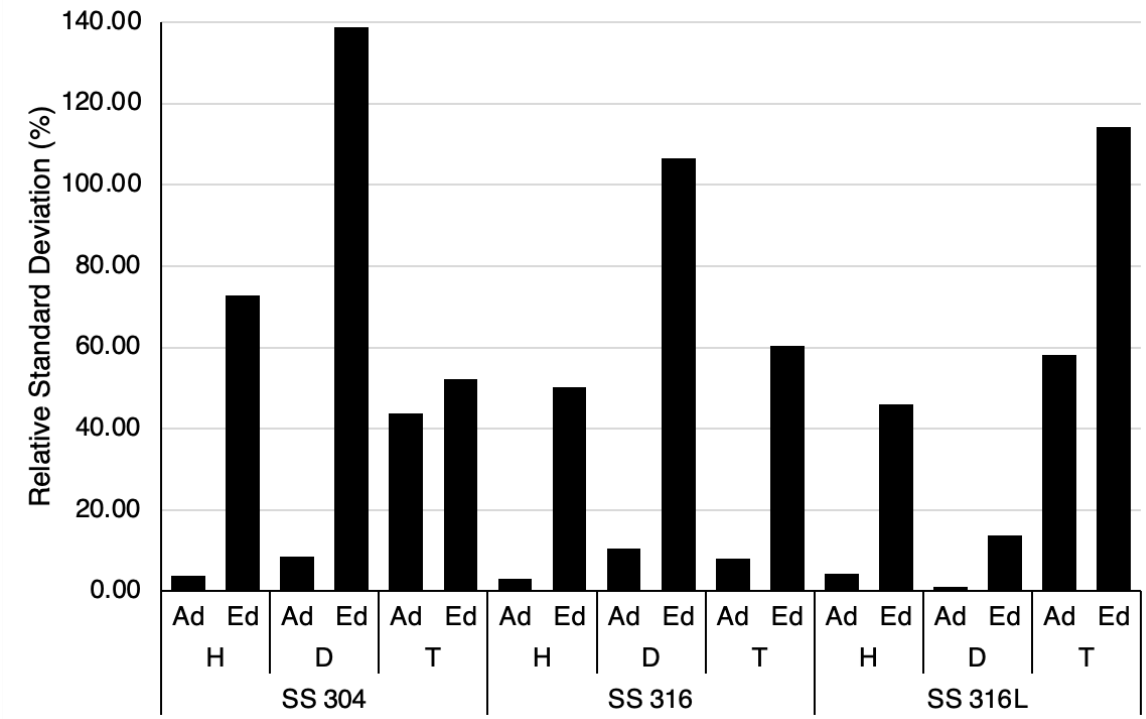

Figure 4. Percent standard deviation of hydrogen isotope diffusion parameters for various stainless steels.

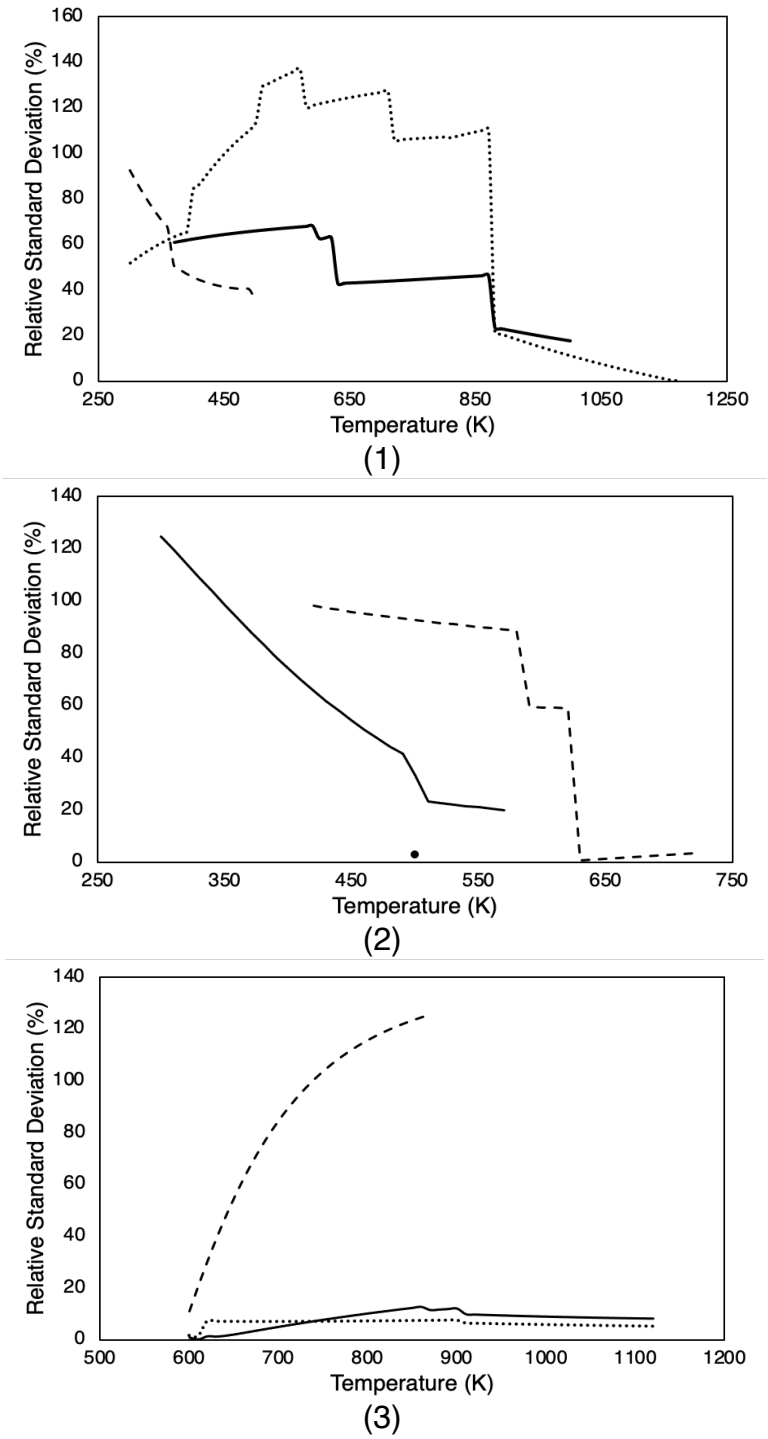

Figure 5. Percent standard deviation of diffusivity of hydrogen isotopes in (1) SS 304, (2) SS 316, (3) and SS 316L with solid, dotted, and dashed lines for hydrogen, deuterium, and tritium respectively.

The Soret effect describes the influence on tritium transport due to a temperature gradient, and the heat of transport parameter defines its impact. From available historical data and calculations based off semi-empirical work for the base metal of stainless steels, Fe, the heat of transport has been estimated to be negative [33, 52, 53]. A study by Longhurst [53] reviewed tritium transport equations accounting for the Soret effect and experimental work conducted to measure the heat of transport in various materials. In this, negative heat of transport values for Fe were determined, and it was approximated that the heat of transport had a linear temperature dependence given by

$$Q^* = a + bT \tag{6}$$

where a and b are constants determined by relating tritium concentrations to pressures using Sieverts' law. The study determined that the Soret effect and its temperature dependence were important in estimating tritium permeation rates of a fusion first-wall structure. In contrast, more recent experimental work by Malo et al. [54] determined a positive heat of transport for SS 316. From this study, it was reported that there is not enough experimental data or theoretical foundation to fully justify assuming a negative heat of transport. As such, further work into determining the heat of transport in steels is necessary. For the work conducted in this thesis, however, the heat of transport used was from a report by Dolan et al. [33] with a value of -6271 J/mole. Temperature dependence reported by Longhurst [53] was neglected since the Soret effect implemented in BISON considers the heat of transport as a constant.

Figure 6 presents an example for how a negative heat of transport and the diffusion coefficient would influence tritium transport. In this, the primary coolant has a higher temperature than the secondary coolant. Therefore, the temperature gradient across the steel has decreasing temperature from left to right. With a tritium source at the left boundary, the direction of the concentration and temperature gradients would the same. A negative heat of transport would mean the Soret effect works from cold to hot temperatures, and thereby, introduces a force on tritium within the example steel from right to left. The concentration gradient introduces a force on tritium within the steel from high to low concentrations, and hence, from left to right. This would result in Fick's diffusion and the Soret effect working in opposite directions.

Tritium Behavior in Fission Systems

Tritium considerations of fission reactors generally focus on radiation safety due to its ever present production, though, its use as fuel in fusion reactors also drives reactor design examination [9, 10, 16-19, 55-57]. Produced tritium in the fuel is typically retained. Though, there are conditions where tritium in the primary coolant becomes a concern whether due to atypical tritium release from fuel regions due to material decisions or production in the coolant. The current main source of commercial tritium is from CANDU fission reactors where the majority of tritium is generated as a result of fission neutrons interacting with the heavy water moderator and coolant. With the development of fusion reactors comes large uncertainty in the availability of tritium, and hence, developing more sources of tritium may be necessary.

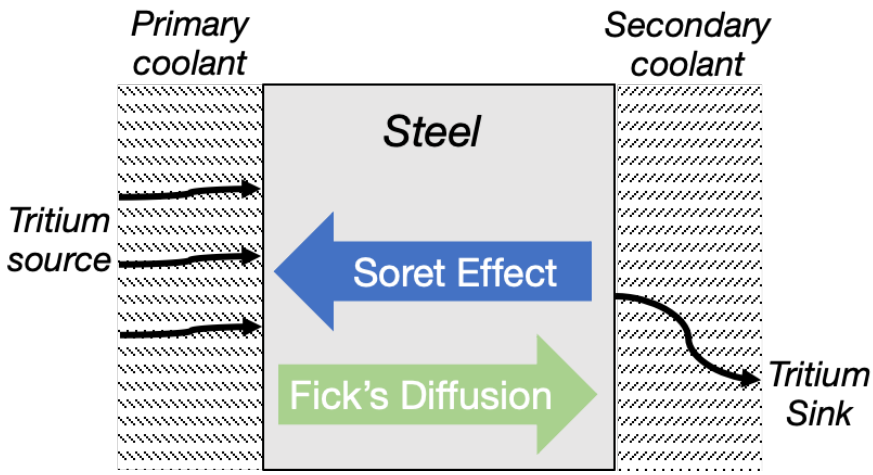

Figure 6. Schematic of BISON models of steel components.

Several studies have been conducted to predict tritium behavior in nuclear fission reactor systems. A study by Ustinov et al. [18] investigated tritium behavior in fast reactors with nitride fuel. Tritium retention occurs within the fuel and may be the result of tritium binding to fission products in the fuel region. Additionally, steel cladding allows for the majority of produced tritium to easily permeate through and into the primary coolant. As tritium diffuses through the steel cladding, some tritium atoms can enter trap sites, and thereby, tritium can result in degrading the physical properties of steel. This results in the need to consider tritium behavior in reactors which utilize steel as cladding to ensure the metal does not degrade to where fuel failure can occur. Additionally, with tritium readily permeating through steel cladding more so than zircaloy, the use of tritium barriers or other tritium control mechanisms may become necessary [17].

Park et al. [55] analyzed tritium transport and permeation behavior through a steel heat exchanger wall of a high temperature gas cooled reactor (HTGR) in a 1D diffusion model. They accounted for tritium diffusion inside the material including impact from a temperature gradient on diffusivity, and determined tritium source as a boundary condition through a balance between solubility which was determined through Sieverts' law and diffusivity in the metal wall. The study was able to accurately predict tritium permeation through steel heat exchanger walls by calculating effective diffusivity using an effective temperature, which revealed the significance of high-fidelity thermal analysis coupled to tritium transport modeling.

Guillou et al. [56] aimed at examining tritium behavior due to temperature in CO_2-cooled nuclear fission reactors also called uranium natural-graphite-gaz (UNGG). To do

this, deuterium was implanted into graphite, and Nuclear Reaction Analysis (NRA) at millimetric and micrometric scales was used to analyze its behavior. The graphite samples were subjected to high vacuum and inert Ar gas flow for temperatures ranging from 200 to 1200°C. Release of deuterium for the graphite sample was mainly driven by its thermal migration and release through its porous structure, and was found to occur from about 400-600°C. For the Saint-Laurent A2 (SLA2) reactor, it was extrapolated that thermal release of tritium due to reactor shutdown which had operated for 11 effective full-power years should be lower than 30% of the amount produced during reactor operation. Additionally, it was concluded that removal of all tritium would be more efficient in dry inert gas with temperatures greater than 1300°C. As tritium retention in irradiated graphite waste contributes significantly to its initial radiological activity, understanding tritium release behavior from graphite can inform reactor design, operation, and waste management.

Tritium Behavior in Breeding Blankets

Commercial fusion reactors utilize tritium as fuel. Due to its natural scarcity and uncertainty in current production methods to provide sufficient amounts of tritium for future development of fusion technology, coolant blankets around the core are designed to produce tritium and will need to produce more than the reactor uses [9, 10, 58]. As such, achieving tritium self-sufficiency is an important qualification for future fusion reactors. Additionally, with the use and production of large amounts of tritium, its transport and behavior in reactor designs necessitate safety considerations.

In a study by Pattison et al. [58], tritium transport behavior in a fusion reactor's dual coolant lead lithium (DCLL) blanket was investigated by modeling a single rectangular duct in a magnetic field with a SiC flow channel insert (FCI). The tritium advection/diffusion equations as well as the source terms and trapping were solved using boundary conditions provided by computing the flow field of the PbLi coolant with computational fluid dynamics (CFD) code. The study predicted that tritium was well-retained within the flow channel insert, the majority of tritium loss occurred in the PbLi gap flow, and tritium permeation into the helium coolant outside the RAFM structure was low. The results revealed the significance of low diffusivity of tritium inside SiC FCI, but it did not include thermal analysis that could account for temperature impacts due to the Soret effect on tritium diffusion.

Fukada et al. [59] examined tritium behavior in Pb-Li blanket systems. Coating F82H reduced activity ferrite/martensite (RAFM) steel with a Er_20_3 ceramic film reduced tritium permeation by a factor greater than 10^3. The reduced tritium permeation rate minimizes tritium inventory in the structural steel, and thereby, improving the potential safety of a reactor. Additionally, experiments using a transient permeation method were conducted to determine the solubility, diffusivity, and permeability of hydrogen isotopes in Pb-Li eutectic alloy. From this, the diffusivity of hydrogen was determined to be 1.4 times larger than deuterium.

A study by Wang et al. [60] examined thermal hydraulic behaviors of low pressure purge gas in tritium breeding zones of a helium cooled solid breeder blanket design. In this, a blanket module was modeled in 3D where lithium ceramic pebbles of Li_4SiO_4 with

90% ^{6}Li enrichment was analyzed through the use of computational fluid dynamics (CFD). The blanket's coolant was high temperature helium gas at 8.0 MPa, and low pressure helium purge gas utilized to extract produced tritium was at 0.12 MPa. The study found that the purge gas was able to extract the produced tritium as well as sufficiently removal of deposited power in breeding zones. Though, the purge gas experienced pressure drops up to about 64 kPa and increased with its inlet velocity while decreased with pebble diameter. As purge gas is utilized in extracting tritium from the blanket module, this study highlights the necessity of thermal hydraulic analysis for blanket performance. Furthermore, if tritium transport is taken into account, flow conditions of the purge gas would affect how much tritium is extracted. This would also affect the potential buildup of tritium and the rate at which this occurs in structural materials.

CHAPTER THREE

TRITIUM TRANSPORT MODELING OF STEEL STRUCTURES IN BISON

Determining which reactor components to model was determined by reviewing multiple studies which conducted tritium transport modeling and experimental work. This focused on whether the model would be of a multiphysics environment to assess the ability of BISON to predict tritium transport in this environment, and thereby, assess the coupling of tritium transport in BISON with other models. Hence, different studies with constant and gradient temperature conditions were decided as necessary. Additionally, to assess the analysis capability of the code for expected reactor operation, studies with steady state and transient tritium conditions were chosen.

The simulations in this thesis are of component-level steel structures where the physical phenomena considered are the diffusion of tritium due to a concentration gradient and the temperature gradient. The concentration gradient drives tritium from higher to lower concentrations, and the Soret effect for steels drives tritium from colder to warmer temperatures. Two of the simulations which are of a LWR fuel pin and FHR heat exchanger have a tritium current into the steels as a boundary condition where temperatures are also hotter at one end of the steel structure compared to the other [12, 13]. Hence, tritium diffusion within these simulations have opposing forces. The remainder simulation also has a tritium current boundary condition, though, the temperature is constant across the structure meaning there is no impact by a temperature gradient [11]. The key figures of merit for these simulations are the tritium distribution and

evolution with time from which the total concentration and permeation rate can be calculated.

A 2D mesh with elements along the x-axis and y-axis were used for all cases, but the temperatures and concentration fields along the y-axis are assumed to be constant. Therefore, these models were essentially 1D models, and Figure 6 can be referred to as depiction of their geometry. For the heat exchanger models, the primary coolant provides the left boundary tritium concentration and the secondary coolant acts as a tritium sink. In regards to the LWR cladding model, the geometry is essentially the same, however, the primary coolant is instead the fuel pin and gap.

For cases with temperature gradients, the model consists of two scripts where the first one solves the temperature distribution at each mesh point for every time step. The subsequent script uses the solved time dependent temperature distribution to calculate the tritium distribution throughout the steel at each mesh point for every time step. In addition, kernels and material properties were used in the code to evaluate values associated with temperature calculations as well as the tritium transport model. Tritium transport parameters and their nominal values used for modeling these cases are listed in Table 4 following the order they are discussed in this chapter. The heat of transport was assumed the same value for each steel material considered [33]. Tritium transport parameter values for FeCrAl were assumed equivalent to those for tritium in SS 304.

SS 316L Heat Exchanger for ITER

Nakamura et al. [11] studied tritium permeation through heat exchanger tubes

Table 4. Values of tritium transport parameters for steel models in BISON.

Parameter	**Unit**	**SS 316L**	**SS 304**	**SS 316**
Diffusivity Frequency Factor, A_D	m^2/s	5.90×10^{-7}	1.24×10^{-6}	6.32×10^{-7}
Diffusivity Activation Energy, E_D	*J/mole*	52095	56726	47800
Heat of Transport, Q^*	*J/mole*	-6271	-6271	-6271

made of stainless steel under similar conditions to those from ITER (International Thermonuclear Experimental Reactor). The SS 316L heat exchanger tubes had an outer diameter of 6 mm, thickness of 0.5 mm, and length of 0.3 m. Considering all 37 tubes, the total surface area where tritium permeation out into the secondary coolant occurred was 0.2 m^2. Both primary and secondary coolants were held at constant values for temperature at 423 K and for pressure at 0.9 MPa. For the primary coolant, tritiated water was filled inside of the tubes while tritium free water filled the chamber outside the tubes. The tritium diffusion coefficient was estimated to be 5×10^{-13} m^2/s, and the derived tritium permeation rate from the experimental results was 4.2×10^{-3} $Bq/m^2/s$ [11].

A 1D model of a single heat exchanger tub was simulated in BISON code consisting of a single region made of SS 316L where the tritiated water was to the left and the pure water was to the right. As the two coolants had equivalent temperatures, a constant temperature of 423 K was assumed over the metal region. A constant tritium concentration equal to the reported value in [11] was applied at the left boundary. The right boundary tritium concentration was set to zero as it was assumed that tritium which reached the boundary was instantaneously released to the secondary coolant. Figure 7 presents a schematic of this model and conditions modeled in BISON.

The calculated tritium distribution evolution inside the steel wall using BISON is presented in Figure 8. A non-linear distribution was calculated for the steady state model due to weakened diffusion of tritium towards the right end. This resulted from a small diffusion coefficient due to a low temperature field as well as the absence of thermal

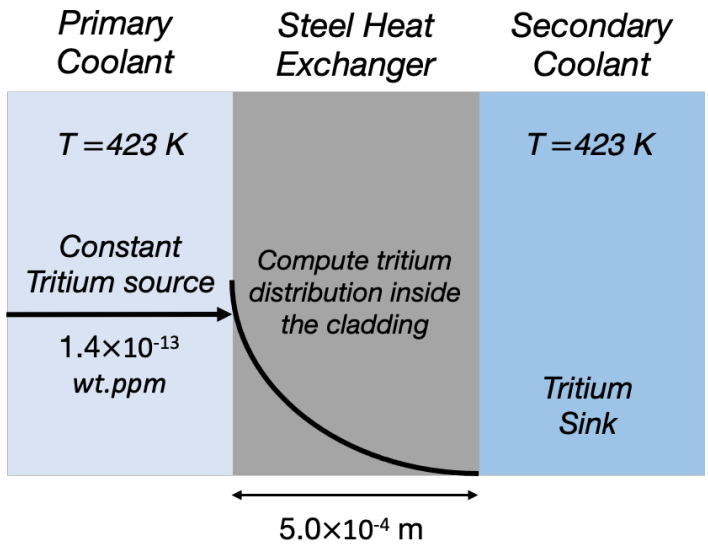

Figure 7. Schematic of ITER heat exchanger tritium transport model in BISON.

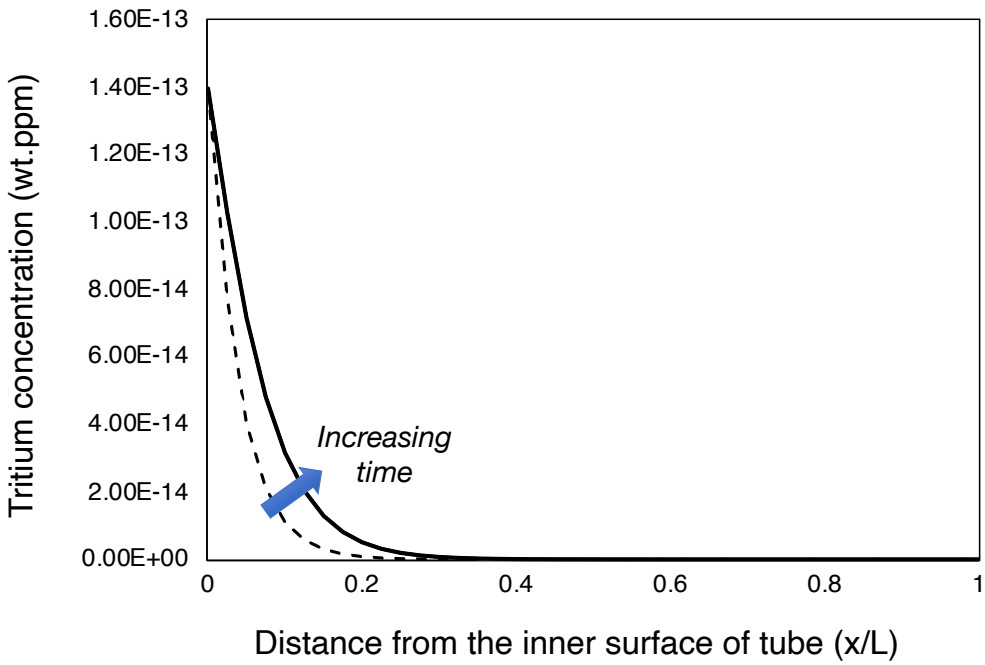

Figure 8. Evolution of tritium distribution across the SS 316L heat exchanger wall.

diffusion. The permeation flux was calculated by utilizing a linear approximation of Fick's first law on the last few spatial nodes of the resulting tritium concentration, and was comparable to the experimental value. BISON's predicted permeation flux of tritium was 1.29×10^{-3} Bq/m^2/s which was on the same order of magnitude as that which is reported in the experiment [11].

FeCrAl Cladding for an LWR

A study conducted by Hu et al. [12] evaluated tritium permeation in iron-chromium-aluminum (FeCrAl) ferritic steel alloy for LWR cladding applications. Hu et al. [12] also reported a simulation of tritium behavior for FeCrAl cladding in a 1000 MW 4-loop PWR using a 1D finite difference method and semi-implicit Crank-Nicolson scheme. Tritium production occurs within the fuel pellets where it then diffuses to and absorbed by the cladding. Further transport of tritium through the cladding to its interface with the primary coolant results in tritium release into the coolant. Fuel operating conditions assume a linear power of 220 W/cm and an 8.22 mm diameter fuel pellet of a LWR 17×17 geometry which result in a power density of 416.6 W/cm^3. This thereby results in a fission rate of 1.26×10^{13} cm^{-3}s^{-1} and a tritium production rate of 1.335×10^{9} cm^{-3}s^{-1}. It was assumed that once the tritium was produced in the fuel, 50% of it was released into the fuel cladding gap. The model accounted for the tritium production rate in the gap, absorption at the inner cladding surface, transport though the cladding structure, and radioactive decay. Absorption of tritium at the cladding surface was determined by Sievert's law where the tritium concentration is proportional to the square root of the pressure in the gap.

Transport and boundary conditions were also defined by diffusion following Fick's laws. The initial concentration throughout the steel cladding was set to zero, and the boundary condition at the interface between the cladding and coolant assumed instantaneous isotope exchange. Hence, tritium is released into the coolant once it reaches this interface.

The model created in BISON code first solved a 1D heat conduction equation for the temperature distribution and then the tritium transport equation with the solved temperature field. This model consisted of three different regions that represented the UO_2 fuel, helium gas gap, and ferritic steel cladding. Figure 9 presents a schematic of the tritium model created in BISON. The primary coolant was included in order to depict the entire considered scenario. A constant volumetric heat source was assumed in the fuel region to match the average temperature of the fuel region reported in [12]. The left boundary was set to be insulated while the right boundary was convective heat transfer to the pressurized water coolant. Figure 10 shows that an appropriate temperature distribution was calculated over all regions. A constant left boundary condition for the tritium source was assumed equal to the approximately steady state tritium concentration reported in [12]. The right boundary condition was set to a concentration of zero to follow the assumption that tritium is instantaneously released to the coolant once it reaches the clad-coolant interface. The BISON simulation then solved the tritium transport equations in the cladding region utilizing the time dependent temperature distribution.

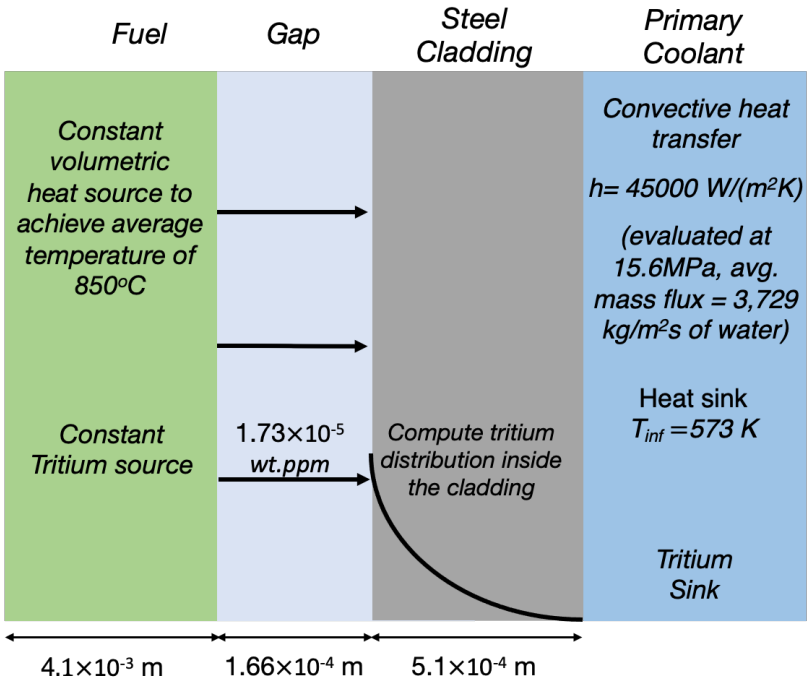

Figure 9. Schematic of tritium transport model in BISON of FeCrAl cladding.

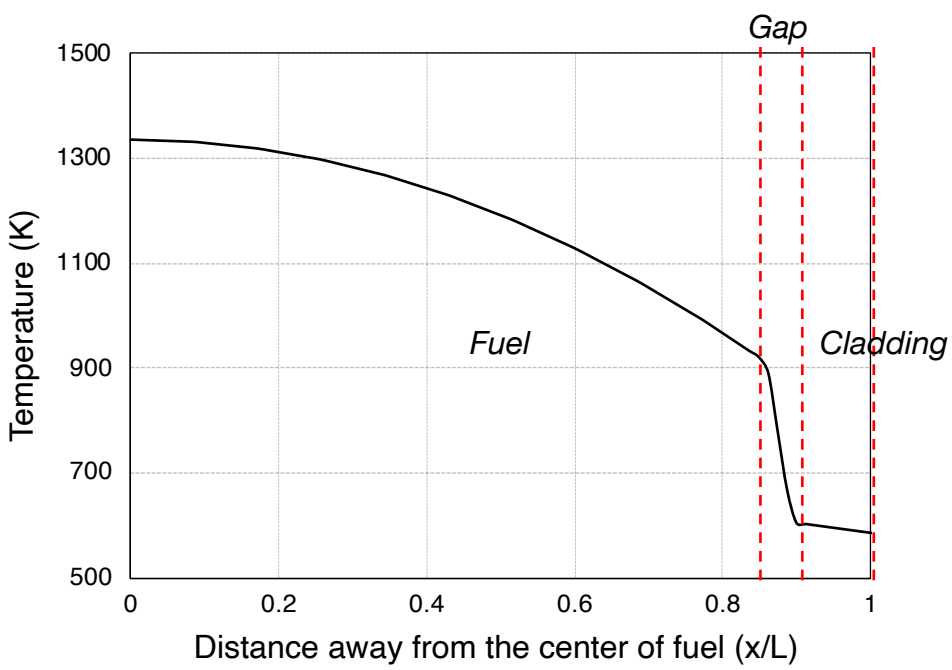

Figure 10. Steady state temperature distribution in the x-direction.

Figure 11 presents the resulting tritium distribution in the cladding predicted by BISON simulation dependent on time and distance from the inner cladding surface. The calculated tritium distribution at steady state is similar to that reported in [12], and Figure 12 shows how model prediction improved as the conditions progressed from transient to steady state. As this model focused on determining comparable results once the model reached steady state, the ability of BISON code to predict tritium distribution in steels under steady state conditions and multiphysics considerations was demonstrated. There are some discrepancies once the model reaches approximately steady state where BISON slightly overpredicts tritium concentration in the center region of the steel.

SS 316 Heat Exchanger for an FHR

Stempien [13] developed a tritium transport model to predict its behavior in a heat exchanger for FHRs during reactor startup. The hot leg SS 316 heat exchanger tubes were approximated as a single pipe with a thickness of 0.02 m, inner diameter of 0.792 m, and length of 29.74 m. Tritium production and accumulation occurs in the FLiBe primary coolant and provided the tritium source boundary condition for the steel wall. In the primary coolant side, the heat exchanger inlet and outlet temperatures were set to be 873.15 K and 973.15 K, respectively. For the secondary coolant, the temperature of 873 K was assumed throughout the secondary loop. The inner boundary balanced tritium fluxes from the bulk coolant to the wall interface and from the wall interface to the metal structure. For the outer boundary condition, it was assumed that tritium was instantly released to the secondary coolant.

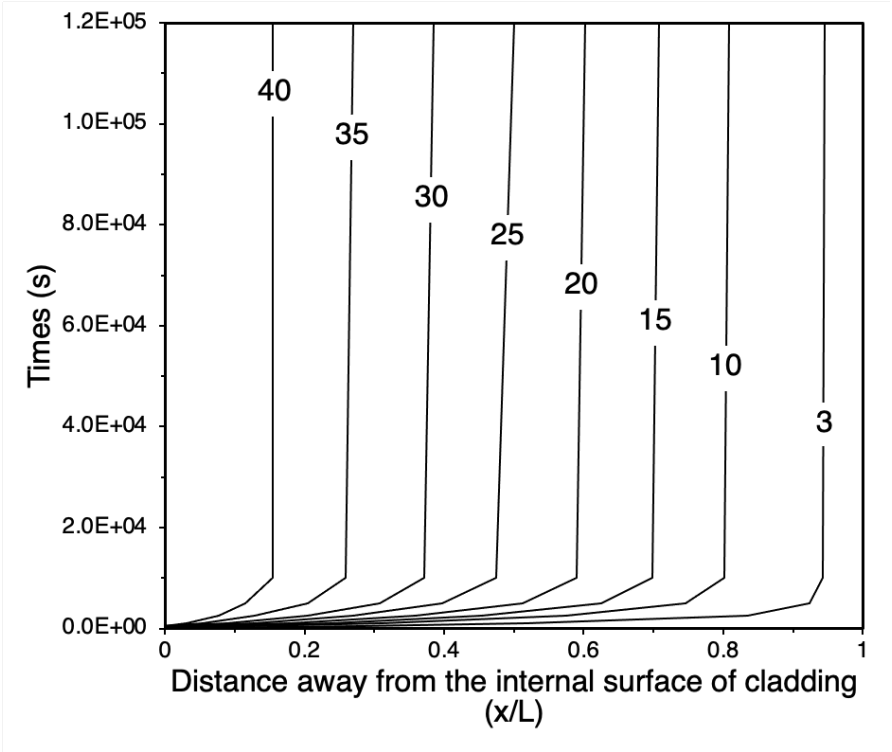

Figure 11. Time evolving tritium distribution in FeCrAl cladding. The numbers in the contour plot are tritium concentration (mol T/cm^3) $\times$ 10^{12}.

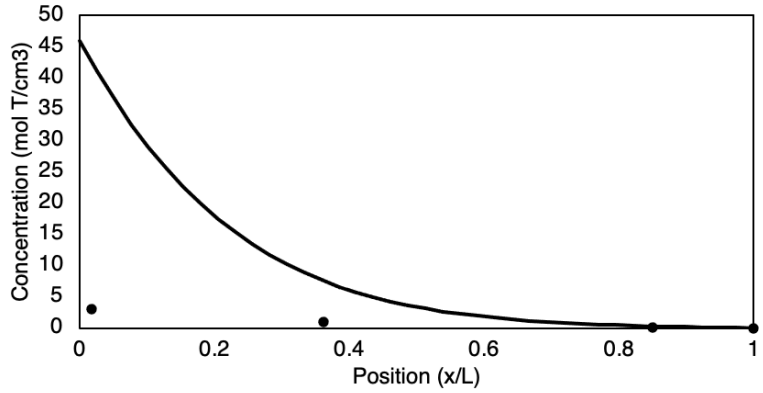

(1)

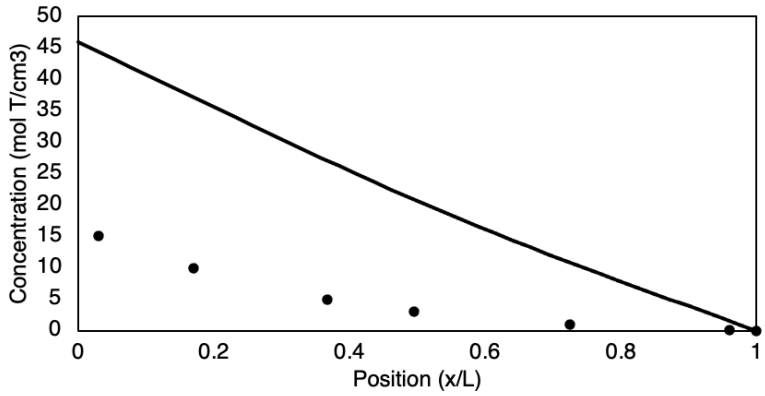

(2)

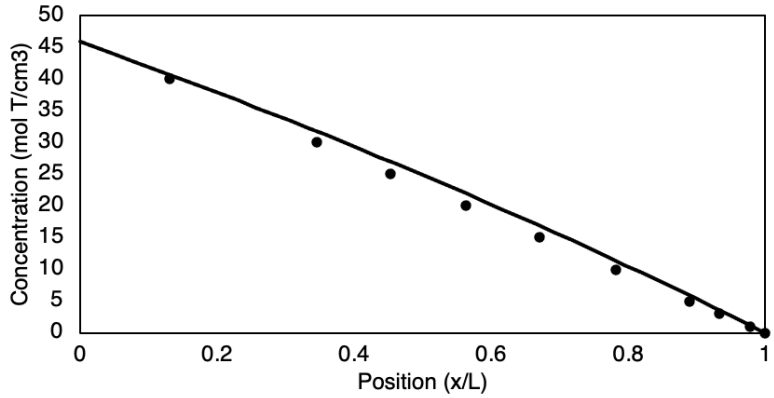

(3)

Figure 12. Tritium distribution in FeCrAl cladding at (1) 1000, (2) 5000, and (3) 120000 seconds. Dotted and solid lines are for reported and BISON results, respectively, and concentrations are times 10^{12}.

The 1D BISON model was divided into two separate steps to calculate heat transfer with convective boundary conditions followed by time dependent tritium distribution. The model, as shown in Figure 13, was of a single 1D metal block with the width equal to the heat exchanger tube's thickness. For the left boundary temperature condition, the coolant temperature was assumed equal to the average of the heat exchanger inlet and outlet temperatures which was about 922 K. The right boundary was set to 873 K. An external data file was made to determine the time-dependent left boundary tritium concentration employing the method reported in [13]. This method essentially balances the amount of tritium within the primary coolant to that in the metal wall by utilizing a set of equations determined from Henry's law, Sievert's law, and Fick's law. To utilize this method, the steel wall was assumed to be a single segment and the centerline tritium concentration was set to be equal to reported values of tritium concentration in the wall. The right boundary condition assumed instant tritium release to the secondary coolant, and therefore, the concentration was set to zero.

Figure 14 shows the predicted concentration of tritium in the steel structure compared to the reported values in [13]. The resulting time dependent tritium concentration calculated by BISON was on the same order of magnitude and followed a similar trend as the reported values, though, BISON overall underpredicted the concentration. This was a result of assuming that the reported values of tritium concentration in the wall were equal to the centerline tritium concentration when determining the transient tritium boundary condition. This is only applicable for steady state conditions where the temperature gradient impacts the tritium concentration. As the

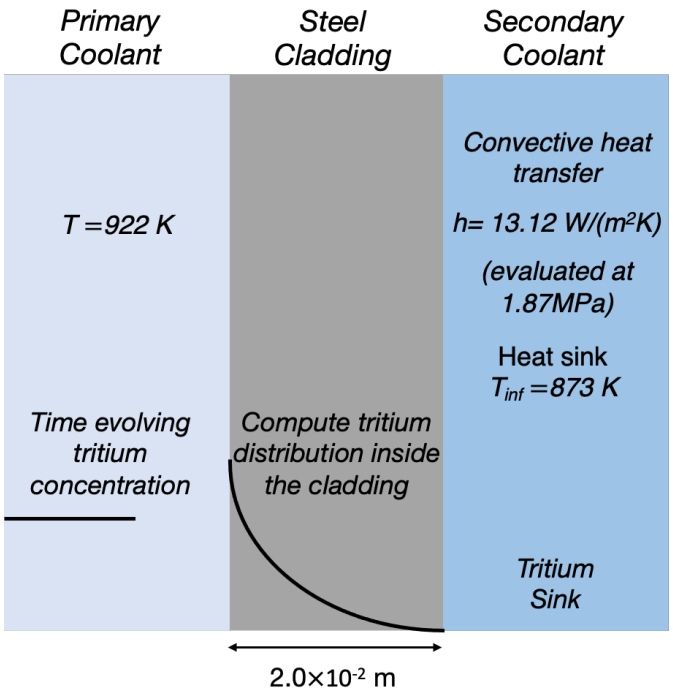

Figure 13. Schematic of FHR heat exchanger tritium transport model in BISON.

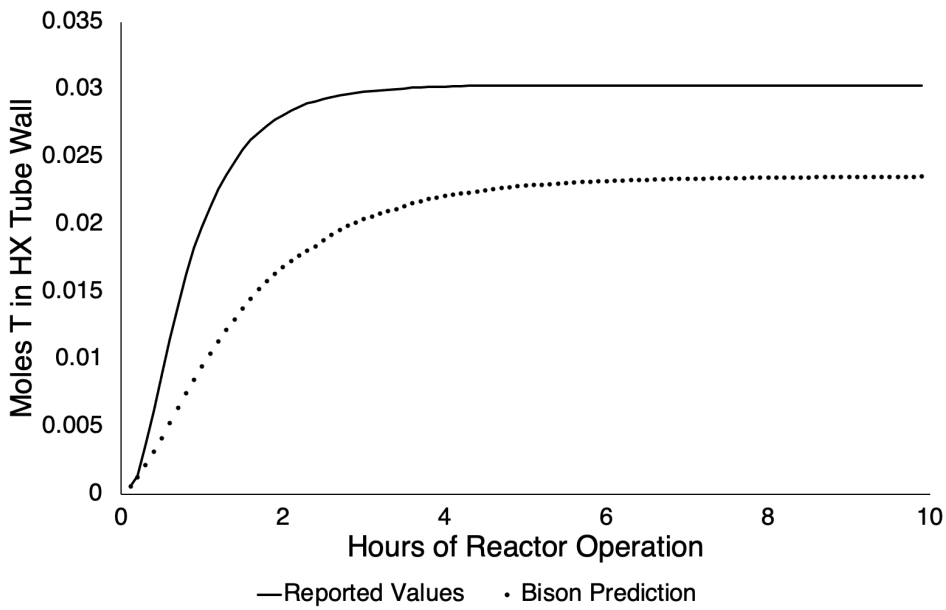

Figure 14. Transient tritium concentration comparison between reported values and BISON predictions.

conditions in the first few hours are a transient, the tritium distribution is more similar to an exponential decay rather than a linear relation, and thereby, result in underpredicting the tritium concentration.

The initial modeling results of three reactor components with varying conditions has demonstrated BISON's ability to predict comparable tritium behaviors across various steel materials. Though, some discrepancies in tritium distribution exist between BISON code predictions and other studies. This might come from the scattered data of diffusion properties of tritium in steel materials, which brought the need of the sensitivity analysis and calibration studies, presented in chapter 4.

CHAPTER FOUR

SENSITIVITY ANALYSIS AND MODEL CALIBRATION

In this chapter, a global sensitivity study of the three steel models is demonstrated as a basis for implementation in a calibration study of a BISON model towards better predictions of tritium transport through steel components. A global sensitivity analysis is used to determine and rank the key input parameters that influence a model's output [61-63]. In this work, Sobol variance decomposition technique was employed for the sensitivity analysis [64]. This technique can account for both linear as well as non-linear correlations, and thereby, is a more general approach to quantify model uncertainties. The first order effect, S_i, from a Sobol analysis represents the contribution a given input has on the output variance and is defined as

$$S_i = \frac{V_{X_i}\left(E_{X_{\sim i}}(f(X)|X_i)\right)}{V(f(X))} \tag{7}$$

where $V(f(X))$ is the variance of $f(X)$, and $E_X(f(X)|X_i)$ is the conditional expected value of $f(X)$ for a fixed input value X_i. Also, a total effect is determined which captures higher order influence in addition to the first order effect, and therefore, represents the contribution to output variance due to interaction with several variables. The total effect, T_i, is defined as

$$T_i = \frac{E_{X_{\sim i}}\left(V_{X_i}(f(X)|X_{\sim i})\right)}{V(f(X))} \tag{8}$$

where $E_{X_{\sim i}}\left(V_{X_i}(f(X)|X_{\sim i})\right)$ is the mean of $f(X)$ for all possible values of $X_{\sim i}$ while holding X_i constant.

A confidence interval below 0.05 ensures that calculated Sobol indices were converged. Total $N * (2D + 2)$ different BISON input decks were generated by the sampler for the Sobol analysis where N is a chosen sample number and D is the number of parameters. Once all cases have been completed, the Saltelli's scheme was used [65] to compute Sobol indices for a chosen Figure of Merit (FoM).

Sobol sensitivity analysis of the three studies previously modeled in BISON was conducted to verify the significance of the impact of diffusion parameters to the prediction as well as to incorporate the ability to calibrate these models. The parameters included in the sensitivity analysis were relevant model parameters for tritium diffusion within steel structures. As such, three input parameters analyzed were the pre-exponential factor for the diffusion coefficient, the diffusion activation energy, and the heat of transport. Ranges of the model parameters were chosen based off literature review and are listed in table 5. The range was estimated to be 40% from the nominal value of reported diffusion parameter values as from Figure 5, the standard deviation of the diffusion coefficient showed larger variance depending on which hydrogen isotope, steel, and temperature were considered. Also, Figure 4 showed the pre-exponential or diffusivity frequency factor varied greatly, from about 14% to 139%, and the largest standard deviation of the activation energy was around 44% and 58%. Therefore, 40% was chosen since the

Table 5. Major parameter variation ranges for Sobol sensitivity analysis.

Material	Parameter	Unit	Lower Bound	Upper Bound
SS 316L	Diffusivity Frequency Factor, A_D	m^2/s	3.54×10^{-7}	8.26×10^{-7}
	Diffusivity Activation Energy, E_D	*J/mole*	31257	72933
SS 304	Diffusivity Frequency Factor, A_D	m^2/s	7.44×10^{-7}	1.74×10^{-6}
	Diffusivity Activation Energy, E_D	*J/mole*	34036	79416
SS 316	Diffusivity Frequency Factor, A_D	m^2/s	3.79×10^{-7}	8.85×10^{-7}
	Diffusivity Activation Energy, E_D	*J/mole*	28680	66920
	Heat of Transport, Q^*	*J/mole*	-8779	-3763

diffusion coefficient showed large variance, it was within the largest standard deviation for the activation energy, and was within the range for the diffusivity frequency factor.

The model calibration study using the results from the sensitivity analysis is presented in this chapter to demonstrate this approach as a basis for implementation in a more comprehensive study of a component-level multiphysics fission reactor component or fusion blanket system. Root Mean Square Error (RMSE) values were calculated for each sample of the sensitivity study and is defined as

$$RMSE = \sqrt{\frac{1}{n}\sum(\hat{y}_i - y_i)} \tag{9}$$

where $\hat{y}_i$ are predicted values and y_i are expected values. Note than an RMSE value is always positive, and the closer it is to zero means that the predicted values more closely match expected values. As such, the calibration study looked for the lowest RMSE value between all samples to determine the parameter values which result in improved model prediction.

In this study, the key FoM of the three cases was the tritium distribution and evolution with time inside the steel structures. Once all sampled BISON input decks ran, a RMSE analysis was implemented in the Sobol sensitivity analysis to calibrate the models. Calculated RMSE values for each case compared values of tritium permeation rate at steady state for the ITER SS316L heat exchanger model, tritium concentration distribution at steady state for the LWR FeCrAl cladding model, and overall tritium

concentration evolving with time in the steel structure for the FHR SS316 heat exchanger model. The RMSE values were then used to calculate Sobol indices.

Figure 15 presents the computed Sobol indices for their respective cases. While the activation energy for the diffusion coefficient had the largest contribution for all three cases, there is slight variation between the calculated indices. In regards to the heat of transport, it did not contribute to the outputs in the first benchmarking case where no temperature gradient existed. The second and third cases had temperature gradients, though, the temperature gradient in the second case was comparatively large to that in the third case. For the third case, the calculated tritium influx at the boundary was dependent on the parameters which determine the diffusion coefficient, and hence, resulted in a larger importance of the pre-exponential factor for the diffusion coefficient compared to the second case. Considering the pre-exponential factor for the diffusion coefficient, the first case was influenced the most between the three cases due to the exclusion of the input by the heat of transport.

Calibration of ITER Heat Exchanger Model

For the model of the ITER heat exchanger, calibration was conducted in regards to the tritium permeation rate into the secondary coolant at steady state between reported and BISON predicted values. As shown in Figure 16(1), there is a strong correlation between the diffusivity activation energy and the prediction of the permeation rate of tritium into the secondary coolant. As initial modeling conditions underpredicted the permeation rate compared to reported values, the model parameters should be adjusted

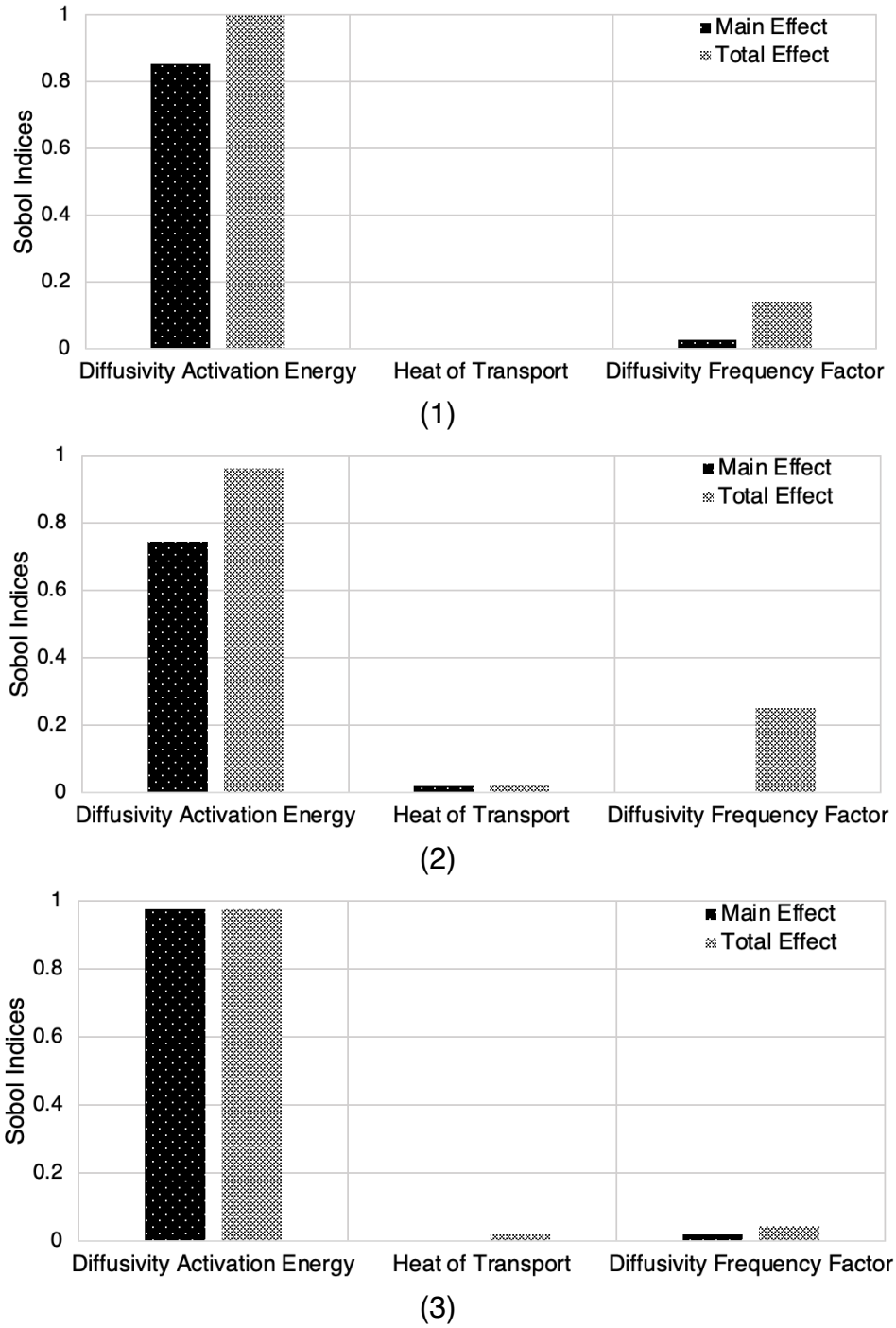

Figure 15. Sobol indices of input parameters for three steel models: (1) ITER SS 316L heat exchanger, (2) LWR FeCrAl cladding, (3) FHR SS 316 heat exchanger.

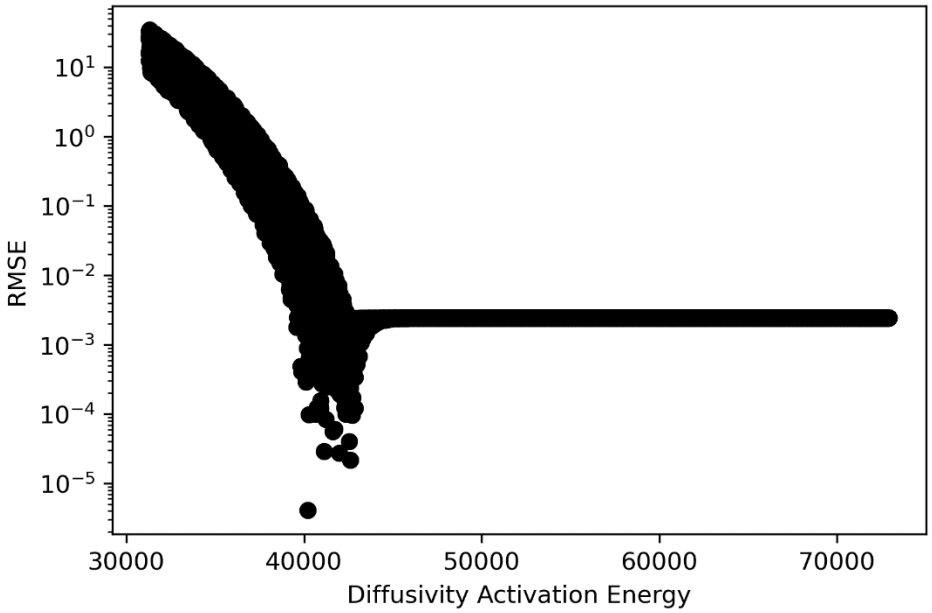

(1)

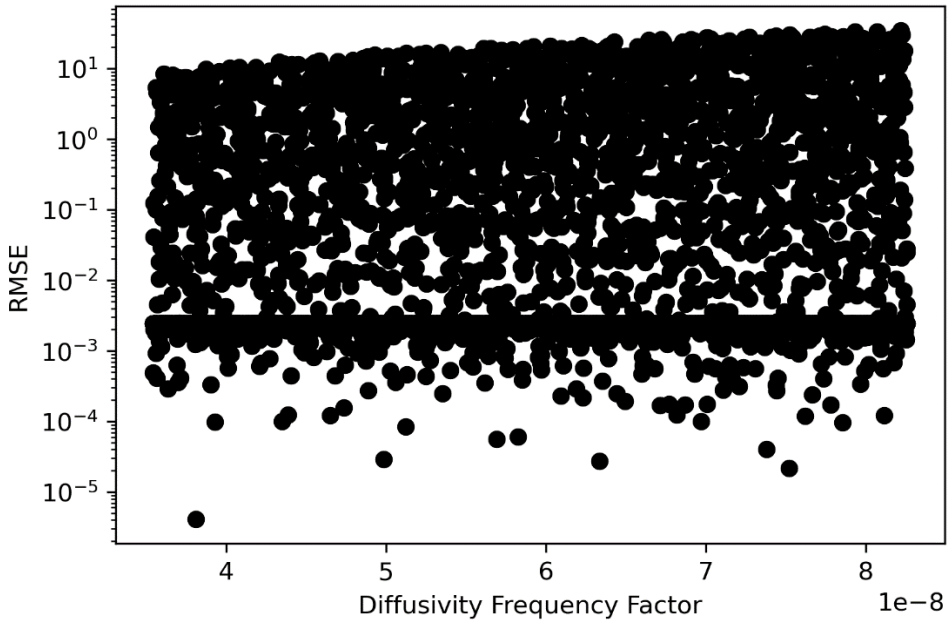

(2)

Figure 16. Scatter plots of RMSE of tritium permeation rate through SS 316L heat exchanger in regards to: (1) diffusivity activation energy, (2) diffusivity frequency factor.

to increase the amount of tritium diffusing through the steel. Considering the influence diffusivity activation energy has on the diffusion coefficient and subsequently tritium transport through steel as a whole, increasing activation energy reduces the amount of tritium diffusing from high concentrations to low concentrations. As such, the trend in Figure 16(1) which shows smaller values of the activation energy from the nominal value result in smaller RMSE values, thereby improved comparative prediction, was expected. Additionally, once the activation energy decreased below about 40000, modeling predictions worsened significantly due to overprediction of the tritium permeation rate.

Figure 16(2) presents the RMSE values in regards to the diffusivity frequency factor and shows two noticeable weaker trends compared to the activation energy. Again considering tritium diffusion as a whole, the trend regarding large RMSE values comes from cases in which the activation energy was too small. This shows worsening model predictions with increasing diffusivity frequency factor, and thereby, both diffusion parameters were resulting in overpredicting the permeation rate. In regards to the trend with smaller RMSE values, these frequency factor values pertain to cases with activation energies that were too large. Though increasing the diffusivity frequency factor in these cases would increase the tritium permeation rate, the permeation rate was more dependent on the activation energy. As such, the best model prediction was made with a frequency factor smaller than the nominal value since the activation energy was sufficiently smaller than its nominal value. A set of diffusion parameters given by the minimum RMSE sample resulted in a calibrated prediction of the tritium permeation rate of 4.19×10^{-3} Bq/m^2/s whereas the reported value was 4.2×10^{-3} Bq/m^2/s.

Calibration of LWR Cladding Model

The calibration of the LWR FeCrAl cladding model determined RMSE values between reported and BISON predictions of tritium concentration distribution once steady state was established. Figure 17 presents the scatter plot of RMSE values pertaining to tritium distribution with regards to the diffusivity activation energy. There is no noticeable trend other than a more populated region of smaller RMSE values at larger activation energies. Also, note that the y-axis scale in Figure 17 was very small, orders of magnitude smaller than in Figure 16. A potential explanation for this is since the analysis for this case focused on tritium distribution at well-established steady state conditions, variations of the activation energy and other transport parameters considered in BISON had little impact on model predictions. As such, there exists some correlation between the diffusivity activation energy and RMSE values, though, there are cases throughout the range of the considered parameter with comparatively small RMSE values. This thereby reveals that the sensitivity to the other parameters can produce a relatively significant difference in model predictions for well-established steady state conditions.

Figure 18 presents the results from inputting the parameter values which lead to the case with the smallest RMSE value back into the model. As the BISON model and calibration method only considered tritium distribution once steady state was established, the min RMSE conditions led to the model in BISON to better match reported results once steady state was established. Figure 19 shows how modeling prediction improved as the conditions progressed from transient to steady state. In regards to the reported transient, the BISON model's predictions showed no improvement. Therefore, the modeling

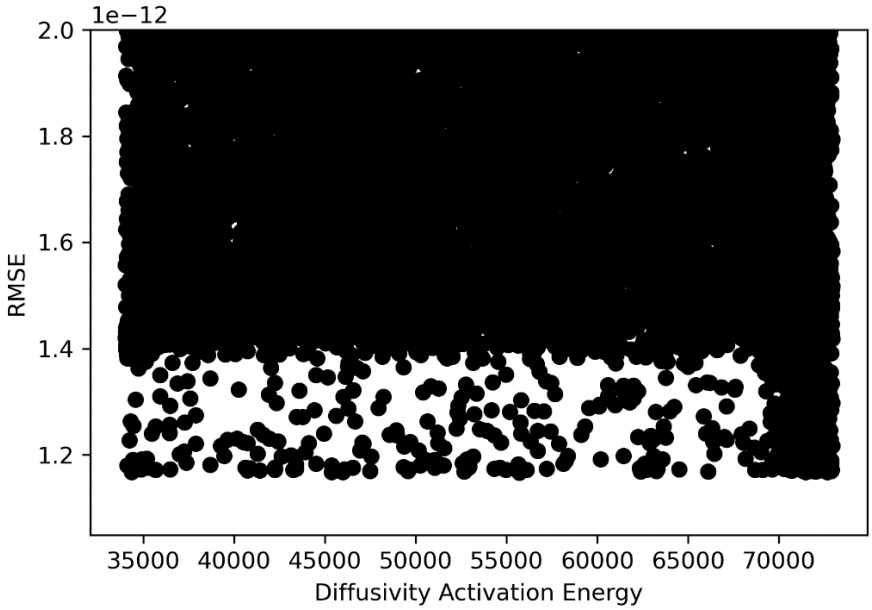

Figure 17. Scatter plot of RMSE of tritium concentration distribution across FeCrAl cladding in regards to diffusivity activation energy.

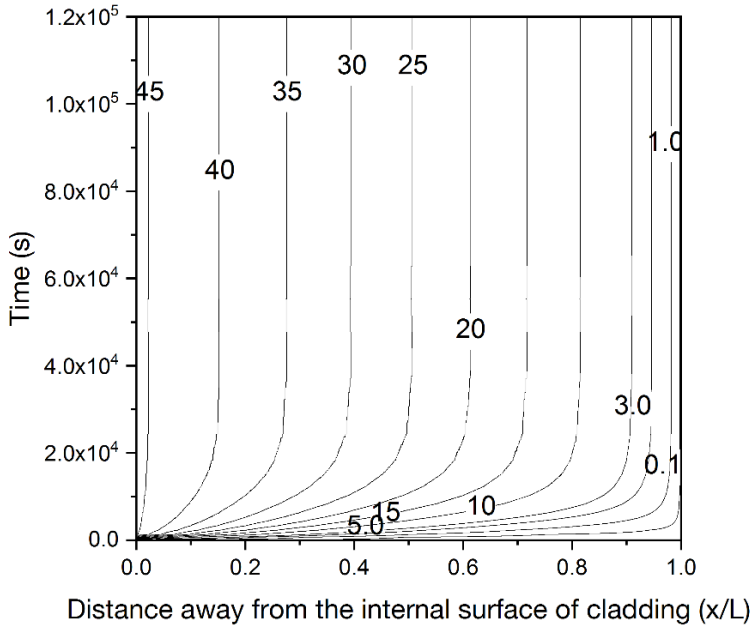

Figure 18. Time evolving tritium distribution in FeCrAl cladding. The numbers in the contour plot are tritium concentration (mol T/cm^3) × 10^{12}.

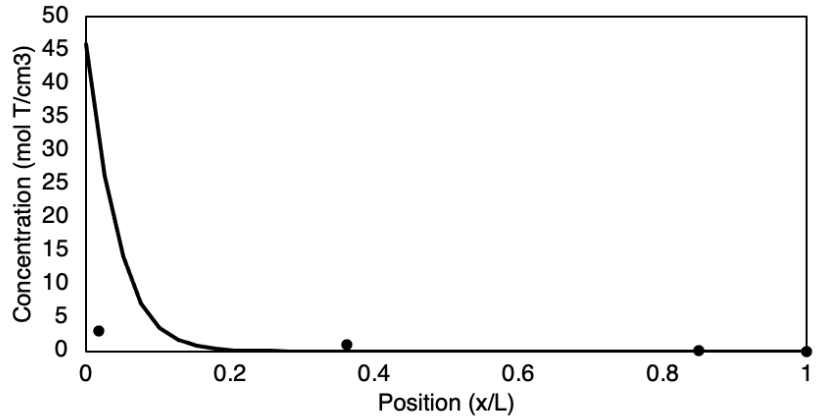

(1)

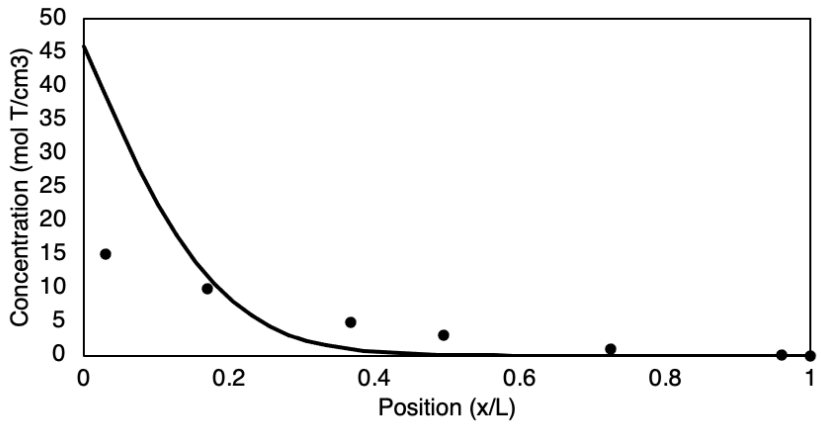

(2)

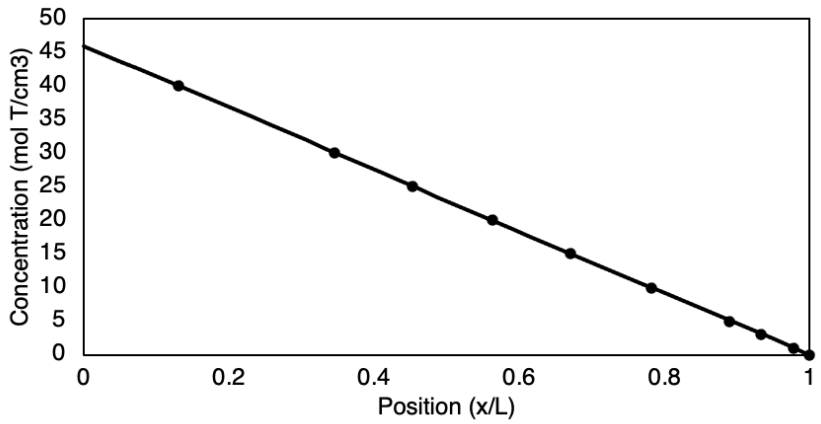

(3)

Figure 19. Tritium distribution in FeCrAl cladding at (1) 1000, (2) 5000, and (3) 120000 seconds. Dotted and solid lines are for reported and BISON results, respectively, and concentrations are times 10^{12}.

decisions and calibration of tritium transport in FeCrAl cladding of a PWR resulted in improving BISON's prediction of tritium behavior once steady state has been established.

Calibration of FHR Heat Exchanger Model

For the calibration of the FHR heat exchanger model, RMSE values were calculated between reported and predicted values of tritium concentration in the wall as time progressed during a transient in which the reactor was started. To account for the transient, all sampled cases were run four times in which all four sets ended at different times. These included three end times over the noticeable transient and one end time once steady state was fully established.

Figure 20 presents the scatter plot of RMSE values in regards to the diffusivity activation energy. The relation between this parameter and tritium concentration in the wall was complicated due to the consideration of the transient. Specifically, the left boundary condition for tritium concentration was dependent on the diffusion coefficient. Decreasing the activation energy and increasing the diffusivity frequency factor increase the diffusion coefficient, and thereby, influence the rate of tritium influx from the primary coolant. From the initial modeling, the rate at which tritium enters the steel the steady state magnitude needed to increase. To calibrate the model which was previously underpredicting, the diffusion coefficient's activation energy was decreased while the diffusivity frequency factor increased. For the heat of transport, its value was decreased as well though this change had little impact on model predictions compared to the diffusivity activation energy.

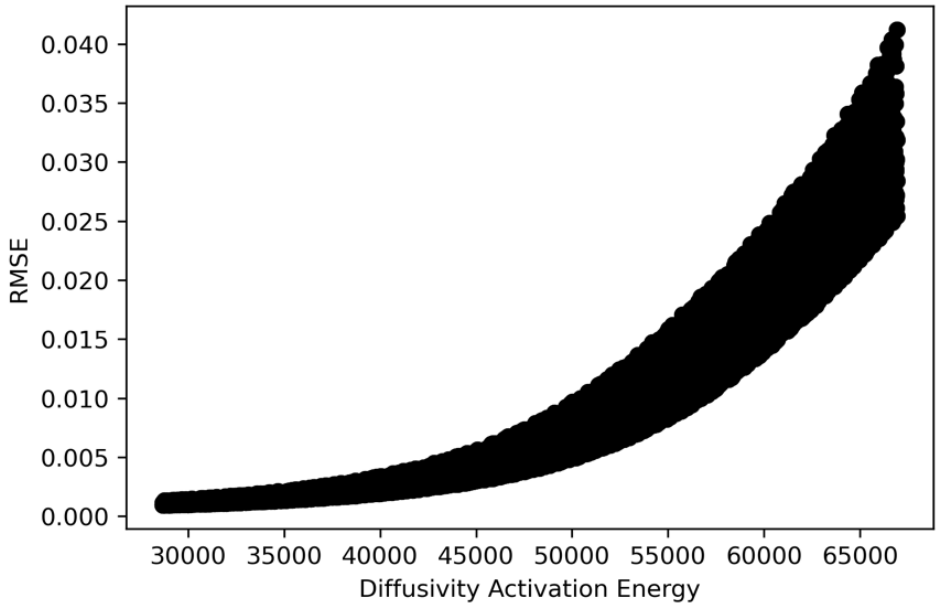

Figure 20. Scatter plot of RMSE of time dependent tritium concentration within a SS 316 heat exchanger tube wall in regards to diffusivity activation energy.

Figure 21 presents the results from the calibrated model. Prediction at steady state and over the transient was improved, though, the model continued slightly underpredicting for the transient. This was a result of the assumptions made in the method to determine the concentration at the left boundary. In this, the method implemented a linear approximation between the concentration at the wall in the steel to the concentration at the center of the steel. Though the implementation of this approximation applies to cases in which the heat of transport was included in simulations, it only applies to steady state conditions. Referring to Figure 8 as a visual aid, tritium concentration follows an exponentially decreasing trend during a transient. Accounting for the heat of transport, this exponential decrease begins to become more linear as the model approaches steady state in this case. As such, the calibrated model slightly underpredicted the transient while matching the steady state value due to the method for determining the boundary condition calculating a smaller influx of tritium than expected. Though, overall BISON demonstrated its ability to predict tritium concentration in steels under transient conditions and multiphysics considerations.

As the resulting BISON prediction which resulted in the smallest RMSE continued to slightly underpredict tritium content during the transient, a variable to adjust the centerline tritium concentration was introduced to the calibration method and referred to as alpha. The variable utilizes the reported tritium content within the metal wall as a maximum value when determining the influx of tritium. This variable ranges from 0.1 to 1.0 where a value of 1.0 would result in matching the previous method. As such, the variable attempts to account for the exponentially decreasing tritium concentration trend

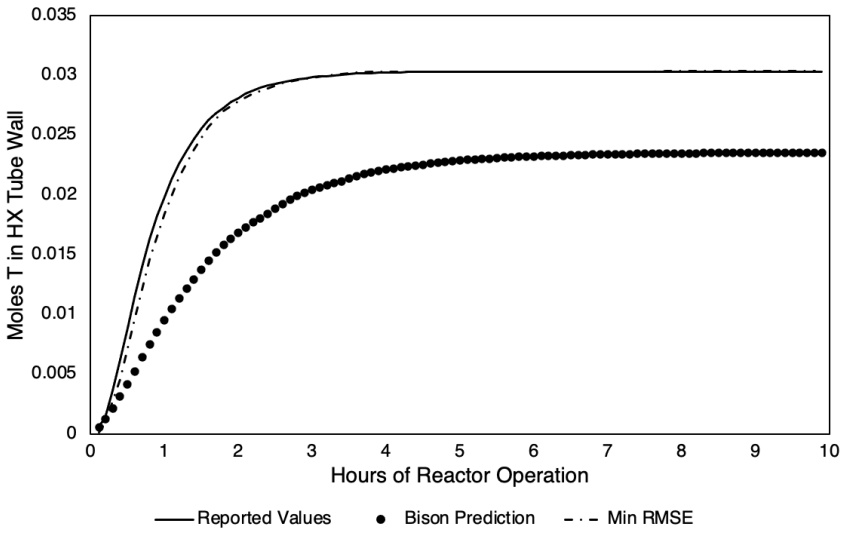

Figure 21. Transient tritium concentration comparison between reported values, initial BISON predictions, and BISON predictions that resulted in the smallest RMSE.

during a transient. The goal of introducing this variable is to determine tritium concentration boundary conditions which better predict tritium concentration in the steel wall over the transient.

Figure 22 presents the computed Sobol indices of the three physical parameters and boundary condition variable alpha. The physical parameters notably decreased in their influence on resulting BISON predictions, though, the activation energy had a comparatively large total effect. This mainly resulted from the interaction of the activation energy and alpha variable on the predicted tritium content. Scatter plots of these two parameters and calculated RMSE values presented in Figure 23 show how these parameters influence predicted tritium concentration. From this, a calibrated alpha variable can be determined. Figure 24 presents the improved model prediction due to introducing the alpha variable. In this, the prediction of tritium concentration during the transient slightly improved, though, the prediction at steady state slightly overpredicted. This was a result of the calculated RMSE values weighing tritium concentrations over the transient more than at steady state due to the distribution of end times for the four sets of sampled cases. Three were centered over the noticeable transient and only one was at a later time for considering steady state. From this, the influence and impact on BISON predictions reveal the need for accurate boundary condition information especially for transients.

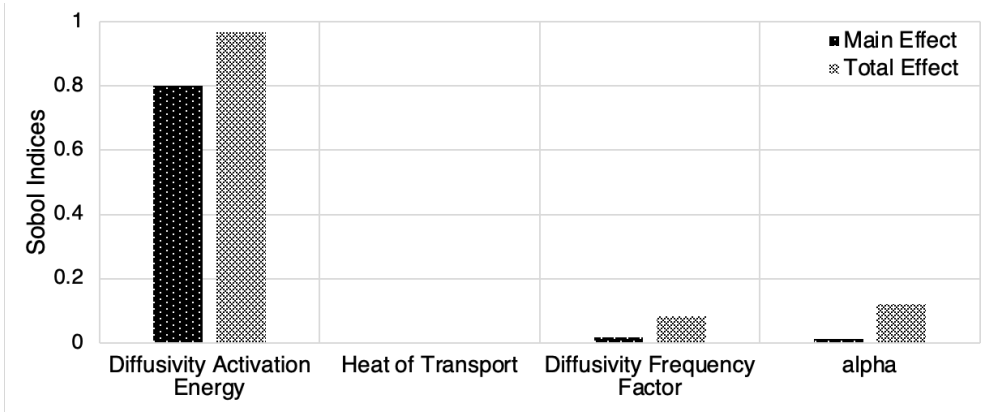

Figure 22. Sobol indices of sampled parameters for FHR heat exchanger model with variable alpha boundary conditions.

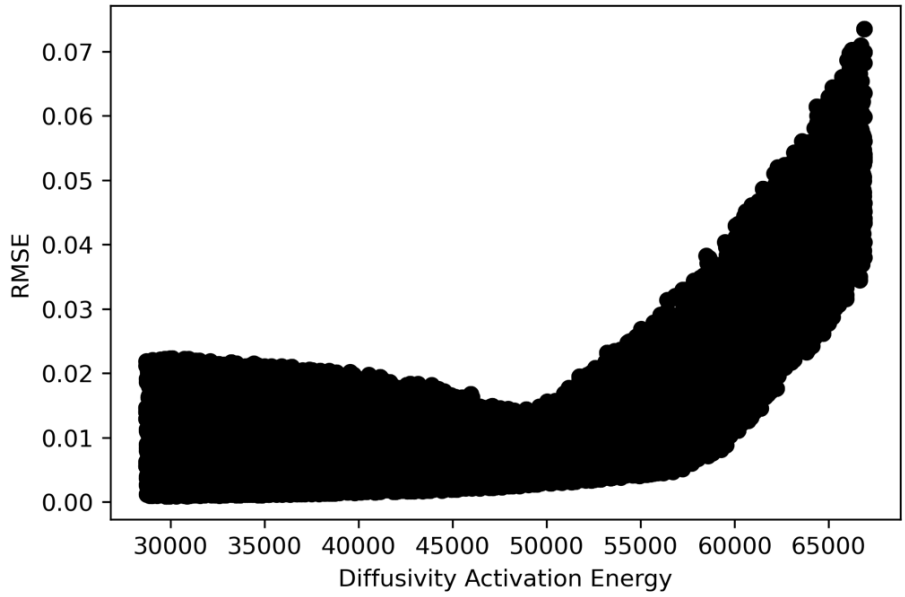

(1)

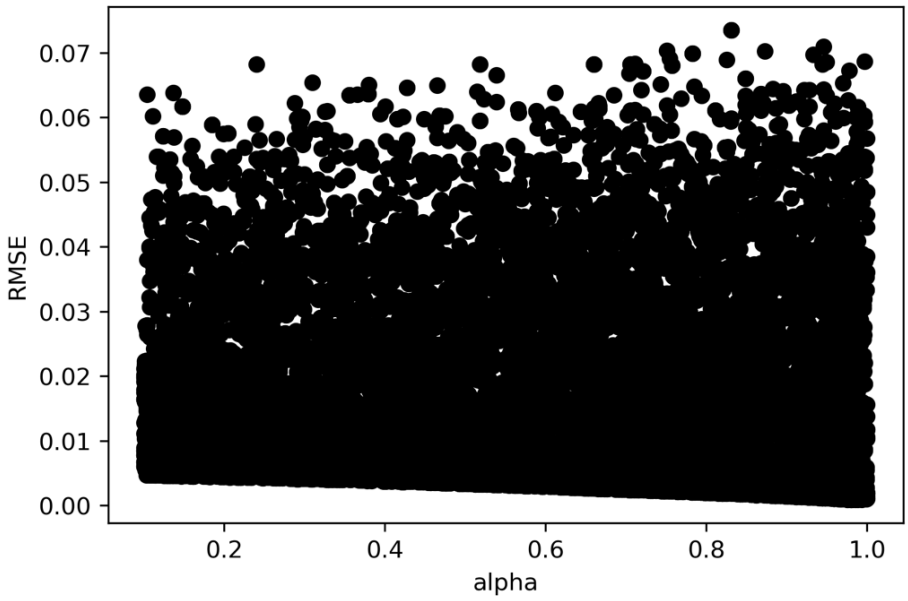

(2)

Figure 23. Scatter plots of RMSE of time dependent tritium concentration within a SS 316 heat exchanger tube wall with variable alpha boundary conditions in regards to: (1) diffusivity activation energy, (2) alpha.

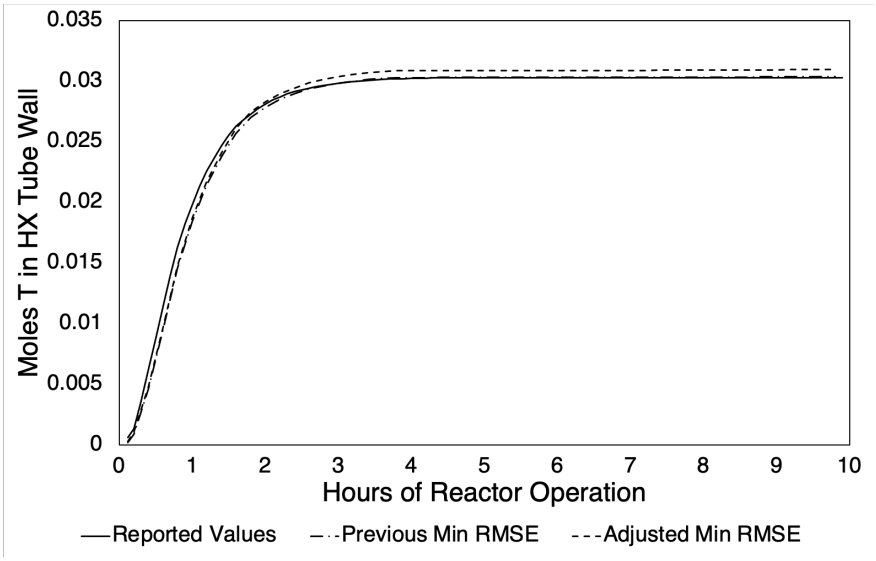

Figure 24. Transient tritium concentration comparison between reported values, initial minimum RMSE, and improved minimum RMSE BISON predictions.

CHAPTER FIVE

CONCLUSIONS

Tritium transport behavior is a primary concern for designs of fusion blanket systems for a commercial fusion reactor as well as a safety concern for fission reactors. Understanding and predicting tritium behavior is important to achieve tritium self-sufficiency as well as mitigate the introduction of this radioactive isotope to the outside environment. To account for multiple physical phenomena and the important information that can be determined from them such as energy extraction in the coolant system, the BISON hydrogen migration and redistribution model was assessed for component-level simulations of tritium transport. This analysis was conducted due to the ability of BISON to be readily coupled with other modeling codes such as MCNP and RELAP5-3D. Information from these codes such as tritium production and coolant flow conditions influence tritium transport behavior, and hence, can inform boundary conditions of a BISON model. Additionally, BISON has the ability to model complex 3D components, and thereby, has the ability to predict tritium behavior in a coupled multiphysics model for many different reactor component designs. Therefore, the work in this paper was conducted to assess BISON's capability to predict tritium behavior in steels as it is a common material for both fission and fusion reactors, and demonstrate a method for model analysis and calibration.

Tritium distribution and evolution with time was modeled for three different systems and conditions. These systems were of a heat exchanger for ITER, cladding for an LWR,

and a heat exchanger for an FHR. Tritium permeation flux through ITER's SS 316L heat exchanger wall was initially predicted to be on the same order of magnitude as the reported value. Predicted tritium concentration within the FeCrAl cladding was similar to reported values at steady state with small overpredictions within the center region of the structure. In regards to an FHR's SS 316 heat exchanger, the time dependent tritium concentration predictions were on the same order of magnitude and followed a similar trend as reported values. Overall, initial simulation results demonstrated the ability of the tritium transport model in BISON to predict comparable results to those from experiments and other models.

A global sensitivity analysis was conducted to demonstrate the ability to extract information of key model parameters as well as demonstrate a method to calibrate model parameters. In this, a Sobol sensitivity analysis was conducted in which a calibration method was implemented through the use of RMSE analysis of model output. In regards to the ITER heat exchanger, predicted tritium permeation rate was calibrated to be within 0.25% of the reported value. The LWR cladding model improved its prediction of tritium concentration in the center region once the model reached steady state. For the FHR heat exchanger model, tritium concentration prediction improved for both steady state and over the transient. To improve model predictions for the transient, a fitting variable was added into the method for determining boundary conditions, and Sobol analysis revealed the expected requirement for accurate boundary conditions especially for transient conditions.

In conclusion, the ability for BISON to predict tritium transport behavior in steel components of fission and fusion systems as well as utilize a method for sensitivity analysis and calibration to improve model prediction was demonstrated. Additionally, the ability for BISON to predict tritium transport in steels was verified. Recommended work in further developing the tritium transport model in BISON include implementing the ability to calculate radioactive decay and trapping behavior. This would account for tritium losses for models covering long periods of time as well as the impact of trapping on tritium diffusion which would change over time due to material damage as a result of a nuclear reactor's extreme environment. Also, implementing the ability to account for transport behavior in fluids would expand BISON's capabilities to model coolants and their interface with structural materials. Additionally, further experimental work for determining the heat of transport in steels is necessary as its value has been reported to be both positive and negative, and it has the potential to significantly influence tritium transport behavior depending on a component's temperature conditions.

REFERENCES

[1] J. B. Greenblatt, N. R. Brown, R. Slaybaugh, T. Wilks, E. Stewart, and S. T. McCoy, "The Future of Low-Carbon Electricity," (in English), *Annu Rev Env Resour,* vol. 42, pp. 289-316, 2017, doi: 10.1146/annurev-environ-102016-061138.

[2] J. E. Phillips and C. E. Easterly, "Sources of Tritium," 1980.

[3] R. B. Rebak, "Alloy Selection for Accident Tolerant Fuel Cladding in Commercial Light Water Reactors," *Metallurgical and Materials Transactions E,* vol. 2, pp. 197-207, 2015, doi: 10.1007/s40553-015-0057-6.

[4] D. P. Jackson *et al.*, "A Review of Fusion Breeder Blanket Technology," 1985.

[5] F. A. Hernandez and P. Pereslavtsev, "First Principles Review of Options for Tritium Breeder and Neutron Multiplier Materials for Breeding Blankets in Fusion Reactors," *Fusion Eng Des,* vol. 137, pp. 243-256, 2018, doi: 10.1016/j.fusengdes.2018.09.014.

[6] T. Ihli *et al.*, "Review of Blanket Designs for Advanced Fusion Reactors," *Fusion Eng Des,* vol. 83, pp. 912-919, 2008, doi: 10.1016/j.fusengdes.2008.07.039.

[7] (1996). *DOE. STD 6002-96, Safety of Magnetic Fusion Facilities*.

[8] S. Sherman and T. Thad Adams, "TRITIUM BARRIER MATERIALS AND SEPARATION SYSTEMS FOR THE NGNP," 2008.

[9] R. J. Pearson, A. B. Antoniazzi, and W. J. Nuttall, "Tritium Supply and Use: a Key Issue for the Development of Nuclear Fusion Energy," *Fusion Eng Des,* vol. 136, pp. 1140-48, 2018, doi: 10.1016/j.fusengdes.2018.04.090.

[10] M. Ni, Y. Wang, B. Yuan, J. Jiang, and Y. Wu, "Tritium Supply Assessment for ITER and DEMOnstration Power Plant," *Fusion Eng Des,* vol. 88, pp. 2422-26, 2013, doi: 10.1016/j.fusengdes.2013.05.043.

[11] H. Nakamura and M. Nishi, "Experimental evaluation of tritium permeation through stainless steel tubes of heat exchanger from primary to secondary water in ITER," (in English), *J Nucl Mater,* vol. 329, pp. 183-187, Aug 1 2004, doi: 10.1016/j.jnucmat.2004.04.009.

[12] X. X. Hu, K. A. Terrani, B. D. Wirth, and L. L. Snead, "Hydrogen permeation in FeCrAl alloys for LWR cladding application," (in English), *J Nucl Mater,* vol. 461, pp. 282-291, Jun 2015, doi: 10.1016/j.jnucmat.2015.02.040.

[13] J. D. Stempien and Massachusetts Institute of Technology. Department of Nuclear Science and Engineering., *Tritium transport, corrosion, and Fuel performance modeling in the Fluoride Salt-Cooled High-Temperature Reactor (FHR)*. 2015, p. 398 pages.

[14] S. B. Seo *et al.*, "Sensitivity Analysis of BISON Model for Characterization of Impact of Experimental Parameters on Hydrogen Migration and Redistribution in Zirconium-Based Alloys," *J Nucl Mater,* vol. 550, 2021, doi: 10.1016/j.jnucmat.2021.152941.

[15] S. B. Seo *et al.*, "A Review of Thermal Hydraulics Systems Analysis for Breeding Blanket Design and Future Needs for Fusion Engineering Demonstration Facility Design and Licensing," *Fusion Eng Des,* vol. 172, 2021, doi: 10.1016/j.fusengdes.2021.112769.

[16] B. W. Gainey, "A Review of Tritium Behavior in HTGR Systems," 1976.

[17] A. Strasser *et al.*, "Evaluation of stainless steel cladding for use in current design LWRs. Final Report.," 1982.

[18] O. A. Ustinov *et al.*, "Tritium in Nitride Fuel of Fast Reactors," *Atomic Energy,* vol. 125, pp. 244-249, 2019, doi: 10.1007/s10512-019-00474-9.

[19] S. Zhang, X. Wu, S. B. Shi, X. D. Sun, R. Christensen, and G. Yoder, "A coupled heat transfer and tritium mass transport model for a double-wall heat exchanger design for FHRs," (in English), *Ann Nucl Energy,* vol. 122, pp. 328-339, Dec 2018, doi: 10.1016/j.anucene.2018.08.039.

[20] P. W. Humrickhouse and B. J. Merrill, "Tritium Aspects of the Fusion Nuclear Science Facility," *Fusion Eng Des,* vol. 135, pp. 302-13, 2018, doi: 10.1016/j.fusengdes.2017.04.099.

[21] R. L. Williamson *et al.*, "Multidimensional multiphysics simulation of nuclear fuel behavior," (in English), *J Nucl Mater,* vol. 423, no. 1-3, pp. 149-163, Apr 2012, doi: 10.1016/j.jnucmat.2012.01.012.

[22] I. Palermo, I. Fernández-Berceruelo, D. Rapisarda, and A. Ibarra, "Neutronics Assessments Towards a Comprehensive Design of DEMO with DCLL Breeding Blanket," *Fusion Eng Des,* vol. 138, pp. 217-225, 2019, doi: 10.1016/j.fusengdes.2018.11.039.

[23] E. Martelli, A. D. Nevo, P. Lorusso, F. Giannetti, V. Narcisi, and M. Tarantino, "Investigation of heat transfer in a steam generator bayonet tube for the

development of PbLi technology for EU DEMO fusion reactor," *Fusion Eng Des,* vol. 159, pp. 111772-, 2020, doi: 10.1016/j.fusengdes.2020.111772.

[24] O. Courty, A. T. Motta, and J. D. Hales, "Modeling and simulation of hydrogen behavior in Zircaloy-4 fuel cladding," (in English), *J Nucl Mater,* vol. 452, no. 1-3, pp. 311-320, Sep 2014, doi: 10.1016/j.jnucmat.2014.05.013.

[25] D. S. Stafford, "Multidimensional simulations of hydrides during fuel rod lifecycle," (in English), *J Nucl Mater,* vol. 466, pp. 362-372, Nov 2015, doi: 10.1016/j.jnucmat.2015.06.037.

[26] E. Lacroix, A. T. Motta, and J. D. Almer, "Experimental determination of zirconium hydride precipitation and dissolution in zirconium alloy," (in English), *J Nucl Mater,* vol. 509, pp. 162-167, Oct 2018, doi: 10.1016/j.jnucmat.2018.06.038.

[27] Z. Aly, A. Casagranda, G. Pastore, and N. R. Brown, "Variance-based sensitivity analysis applied to hydrogen migration and redistribution model in Bison. Part I: Simulation of historical experiments," (in English), *J Nucl Mater,* vol. 524, pp. 90-100, Oct 2019, doi: 10.1016/j.jnucmat.2019.06.035.

[28] Z. Aly, A. Casagranda, G. Pastore, and N. R. Brown, "Variance-based sensitivity analysis applied to the hydrogen migration and redistribution model in Bison. Part II: Uncertainty quantification and optimization," (in English), *J Nucl Mater,* vol. 523, pp. 478-489, Sep 2019, doi: 10.1016/j.jnucmat.2019.06.023.

[29] S. Lynch, "Hydrogen embrittlement phenomena and mechanisms," (in English), *Corros Rev,* vol. 30, no. 3-4, pp. 105-123, Jun 2012, doi: 10.1515/corrrev-2012-0502.

[30] J. Venezuela, Q. L. Liu, M. X. Zhang, Q. J. Zhou, and A. Atrens, "The influence of hydrogen on the mechanical and fracture properties of some martensitic advanced high strength steels studied using the linearly increasing stress test," (in English), *Corros Sci,* vol. 99, pp. 98-117, Oct 2015, doi: 10.1016/j.corsci.2015.06.038.

[31] A. Sawatzky, "The Diffusion and Solubility of Hydrogen in the Alpha-Phase of Zircaloy-2," (in English), *J Nucl Mater,* vol. 2, no. 1, pp. 62-68, 1960, doi: Doi 10.1016/0022-3115(60)90025-8.

[32] J. J. Kearns, "Diffusion-Coefficient of Hydrogen in Alpha Zirconium, Zircaloy-2 and Zircaloy-4," (in English), *J Nucl Mater,* vol. 43, no. 3, pp. 330-&, 1972, doi: Doi 10.1016/0022-3115(72)90065-7.

[33] T. J. Dolan and R. A. Anderl, "Assessment of database for interaction of tritium with ITER plasma facing materials," Idaho National Laboratory, 1994, vol. 26.

[34] T. Tanabe, Y. Yamanishi, K. Sawada, and S. Imoto, "Hydrogen Transport in Stainless-Steels," (in English), *J Nucl Mater,* vol. 123, no. 1-3, pp. 1568-1572, 1984, doi: Doi 10.1016/0022-3115(84)90304-0.

[35] N. Kishimoto, T. Tanabe, T. Suzuki, and H. Yoshida, "Hydrogen Diffusion and Solution at High-Temperatures in 316L Stainless-Steel and Nickel-Base Heat-Resistant Alloys," (in English), *J Nucl Mater,* vol. 127, no. 1, pp. 1-9, 1985, doi: Doi 10.1016/0022-3115(85)90056-X.

[36] M. Braun, B. Emmoth, F. Waelbroeck, and P. Wienhold, "Determination of Deuterium Surface Recombination Rates on Stainless Steel," *J Nucl Mater,* vol. 93, pp. 861-865, 1980, doi: 10.1016/0022-3115(80)90219-6.

[37] D. M. Grant, D. L. Cummings, and D. A. Blackburn, "Hydrogen in 304 Steel: Diffusion, Permeation and Surface Reaction," *J Nucl Mater,* vol. 149, pp. 180-191, 1987.

[38] E. Hashimoto and T. Kino, "Hydrogen Permeation Through Type 316 Stainless Steels and Ferritic Steel for a Fusion Reactor," *J Nucl Mater,* vol. 133, pp. 289-291, 1985, doi: 10.1016/0022-3115(85)90153-9.

[39] H. Katsuta and K. Furukawa, "Hydrogen and Deuterium Transport through Type 304 Stainless Steel at Elevated Temperatures," *J Nucl Mater,* vol. 18, pp. 143-151, 1981, doi: 10.1080/18811248.1981.9733235.

[40] N. Kishimoto, T. Tanabe, T. Suzuki, and H. Yoshida, "Hydrogen Diffusion and Solution at High Temperatures in 316L Stainless Steel and Nickel-Base Heat-Resistant Alloys," *J Nucl Mater,* vol. 127, pp. 1-9, 1985, doi: 10.1016/0022-3115(85)90056-X.

[41] R. A. Langley, "Hydrogen Trapping, Diffusion and Recombination in Austenitic Stainless Steels," *J Nucl Mater,* vol. 128-129, pp. 622-628, 1984, doi: 10.1016/0022-3115(84)90424-0.

[42] T. Namba, M. Yamawaki, and M. Kanno, "Surface Processes of Hydrogen Transport in Fusion Reactor Materials," *J Nucl Mater,* vol. 128-129, pp. 646-651, 1984, doi: 10.1016/0022-3115(84)90428-8.

[43] T.-P. Perng and C. J. Altstetter, "Effects of Deformation on Hydrogen Permeation in Austenitic Stainless Steels," *Acta Metallurgica,* vol. 34, pp. 1771-1781, 1986, doi: 10.1016/0001-6160(86)90123-9.

[44] F. Reiter, J. Camposilvan, M. Caorlin, G. Saibenea, and R. Sartori, "Interaction of Hydrogen Isotopes with Stainless Steel 316 L," *Fusion Technology,* vol. 8, pp. 2344-2351, 1985, doi: 10.13182/FST85-A24629.

[45] C. Shan, A. Wu, and Q. Chen, "The Behavior of Diffusion and Permeation of Tritium through 316L Stainless Steel," *J Nucl Mater,* vol. 179, pp. 322-324, 1991, doi: 10.1016/0022-3115(91)90091-K.

[46] M. Sugisaki, H. Furuya, H. Ueki, and S. Ejima, "Surface Reaction and Bulk Diffusion of Tritium in SUS-316 Stainless Steel," *J Nucl Mater,* vol. 133, pp. 280-283, 1985, doi: 10.1016/0022-3115(85)90151-5.

[47] K. L. Wilson and M. I. Baskes, "Deuterium Trapping in Irradiated 316 Stainless Steel," *J Nucl Mater,* vol. 76, pp. 291-297, 1978, doi: 10.1016/0022-3115(78)90160-5.

[48] W. J. Byeon, S. K. Lee, and S. J. Noh, "Transport of Hydrogen and Deuterium in 316LN Stainless Steel over a Wide Temperature Range for Nuclear Hydrogen and Nuclear Fusion Applications," *International Journal of Hydrogen Energy,* vol. 45, pp. 8827-8832, 2020, doi: 10.1016/j.ijhydene.2020.01.130.

[49] S. K. Lee, S.-H. Yun, H. G. Joo, and S. J. Noh, "Deuterium Transport and Isotope Effects in Type 316L Stainless Steel at High Temperatures for Nuclear Fusion

and Nuclear Hydrogen Technology Applications," *Current Applied Physics,* vol. 14, pp. 1385-1388, 2014, doi: 10.1016/j.cap.2014.08.006.

[50] S. Naoe, Y. Torikai, R. D. Penzhorn, K. Akaishi, K. Watanabe, and M. Matsuyama, "Transport of Tritium in SS316 at Moderate Temperatures," *Fusion Sci Technol,* vol. 54, pp. 515-5187, 2008, doi: 10.13182/FST08-1.

[51] R. A. Causey, R. A. Karnesky, and C. San Marchi, "4.16 - Tritium Barriers and Tritium Diffusion in Fusion Reactors," *Comprehensive Nuclear Materials,* 2012, doi: 10.1016/B978-0-08-056033-5.00116-6.

[52] M. I. Baskes, W. Brauer, and K. L. Wilson, "Tritium Permeation in Fusion Reactor First Walls," *J Nucl Mater,* vol. 111, pp. 663-666, 1982, doi: 10.1016/0022-3115(82)90286-0.

[53] G. R. Longhurst, "The Soret Effect and Its Implications for Fusion Reactors," *J Nucl Mater,* vol. 131, pp. 61-69, 1985, doi: 10.1016/0022-3115(85)90425-8.

[54] M. Malo, F. J. Valle, F. M. Jimenez, A. Morono, E. R. Hodgson, and C. Moreno, "Hisotope Thermo-Diffusion in Structural Materials," *Fusion Eng Des,* vol. 124, pp. 924-927, 2017, doi: 10.1016/j.fusengdes.2017.01.012.

[55] M. Y. Park, B. J. Kim, and E. S. Kim, "Development of semi-empirical model for tritium permeation under non-uniform temperature distribution at heat exchanger tube wall," (in English), *Ann Nucl Energy,* vol. 75, pp. 413-420, Jan 2015, doi: 10.1016/j.anucene.2014.08.044.

[56] M. L. Guillou, N. Toulhoat, Y. Pipon, and N. Moncoffre, "Deuterium Migration in Nuclear Graphite: Consequences for the Behavior of Tritium in CO2-Cooled

Reactors and for the Decontamination of Irratiated Graphite Waste," *J Nucl Mater,* vol. 461, pp. 72-77, 2015, doi: 10.1016/j.jnucmat.2015.03.005.

[57] S. N. Lee and N.-I. Tak, "Tritium Transport and Distribution in a High-Temperature Gas-Cooled Reactor," *Fusion Eng Des,* vol. 76, pp. 238-245, 2020, doi: 10.1080/15361055.2019.1705725.

[58] M. J. Pattison, S. Smolentsev, R. Munipalli, and M. A. Abdou, "Tritium Transport in Poloidal Flows of a DCLL Blanket," *Fusion Sci Technol,* vol. 60, 2, pp. 809-813, 2011, doi: 10.13182/FST10-309.

[59] S. Fukada *et al.*, "Clarification of Tritium Behavior in Pb-Li Blanket System," *The Japan Institute of Metals and Materials,* pp. 425-29, 2013, doi: 10.2320/matertrans.MG201203.

[60] M. Wang *et al.*, "Numerical study on the purge gas flow and heat transfer characteristices in helium cooled solid breeder blanket CFETR," *Progres in Nuclear Energy,* vol. 105, pp. 114-123, 2018, doi: 10.1016/j.pnucene.2017.12.012.

[61] T. Ikonen, "Comparison of global sensitivity analysis methods – Application to fuel behavior modeling," *Nuclear Engineering and Design,* vol. 297, pp. 72-80, 2016, doi: 10.1016/j.nucengdes.2015.11.025.

[62] A. Saltelli, P. Annoni, I. Azzini, F. Campolongo, M. Ratto, and S. Tarantola, "Variance based sensitivity analysis of model output. Design and estimator for the total sensitivity index," *Computer Physics Communications,* vol. 181, no. 2, pp. 259-270, 2010, doi: 10.1016/j.cpc.2009.09.018.

[63] A. Saltelli, "Making best use of model evaluations to compute sensitivity indices," vol. 145, no. 2, pp. 280-297, 2002, doi: 10.1016/S0010-4655(02)00280-1.

[64] I. M. Sobol, "Sensitivity Estimates for Nonlinear Mathematical Models," *Mathematical Modeling and Computational Experiment,* vol. 1, pp. 407-414, 1993.

[65] J. Herman and W. Usher, "SALib: An open-source Python library for Sensitivity Analysis," *Journal of Open Source Software,* vol. 97, doi: 10.21105/joss.00097.

VITA

Miles L. O'Neal grew up in Texas where after high school, he attended Texas A&M University at College Station and graduated with a Bachelor of Science in Nuclear Engineering in December 2019. Miles began attending the University of Tennessee Knoxville in January 2020 where his anticipated graduation date for his Master of Science is August 2021.